ARTICLE IN PRESS

Progress in Oceanography xxx (2010) xxx–xxx

Contents lists available at ScienceDirect

Progress in Oceanography

journal homepage: www.elsevier.com/locate/pocean

Review

The linear models of the ACC

J.H. LaCasce [a,*], P.E. Isachsen [b]

[a] University of Oslo, Department of Geosciences, P.O. Box 1022 Blindern, 0315 Oslo, Norway
[b] Norwegian Meteorological Institute, P.O. Box 43 Blindern, 0313 Oslo, Norway

ARTICLE INFO

Article history:
Received 24 July 2009
Received in revised form 17 November 2009
Accepted 28 November 2009
Available online xxxx

ABSTRACT

Discussions of the dynamics of the Antarctic Circumpolar Current (ACC) generally focus on eddies. The linear, analytical models are discussed only infrequently, and none of these models has gained widespread acceptance. These models nevertheless exist and exhibit interesting, and often realistic, features. We revisit those models, to understand their dynamics and to assess their relevance to the ACC.

We focus specifically on the steady, linear, wind-driven models, and those with either a barotropic or equivalent barotropic vertical structure. The most important feature distinguishing them is their choice of geostrophic contours (f/H or the equivalent), whether closed or blocked.

We first examine the flat bottom models. With closed geostrophic contours, the solutions have a flow which is primarily along the contours and a transport which is inversely proportional to the bottom drag coefficient. For realistic parameters, this transport is excessively large. Solution with blocked contours instead exhibit gyres, with cross-contour flow and western boundary currents. But they also have one or more circumpolar jets, which follow the geostrophic contours over most of the domain. In contrast to the closed contour models, these jets have a transport which asymptotes to a constant value when the bottom drag is vanishingly weak.

We then discuss solutions with bottom topography, focusing in particular on the equivalent barotropic solution. The central parameter here is the vertical scale of the current, which determines the extent of the interaction with topography and the degree to which the geostrophic contours are blocked. The solutions with a shallow current are less affected by topography and have closed geostrophic contours and large transports. Solutions with too large vertical extent are overly-controlled by topography and exhibit only weak circumpolar transport.

Solutions with an intermediate vertical scale have blocked contours and also reasonable circumpolar transport. Furthermore, these solutions exhibit strikingly realistic surface height fields. As in the flat bottom case, the solutions have an interior in Sverdrup balance and a circumpolar transport which asymptotes with vanishing bottom friction. We demonstrate that this transport can be estimated via a contour integral; the result agrees well with the full equivalent barotropic solution. Both are nevertheless roughly 50% larger than observed in Drake Passage. However, the transport can be reduced to realistic values by adding lateral dissipation to the model.

Thus the equivalent barotropic model is successful at capturing the steering of the ACC by topography, given the vertical scale of the current. However, it remains to understand what determines that scale. Thermohaline forcing and lateral mixing by eddies are likely to be important.

Contents

1. Introduction 00
   1.1. The models 00
2. Equations 00
3. Ishida's model. 00
   3.1. Numerical solutions 00
4. Gill's model. 00
5. Equivalent barotropic model with topography. 00
6. Comparing the EB model to observations. 00

* Corresponding author. Tel.: +47 228 55955; fax: +47 228 55269.
E-mail address: j.h.lacasce@geo.uio.no (J.H. LaCasce).

0079-6611/$ - see front matter © 2009 Elsevier Ltd. All rights reserved.
doi:10.1016/j.pocean.2009.11.002

6.1. Lateral diffusion 00
6.2. Wind stress curl 00
7. Comparing the EB model to GCMs 00
7.1. Form drag 00
8. Summary and discussion 00
Appendix A. 00
References 00

1. Introduction

Conventional wisdom states that the dynamics of the Southern Ocean are like those of the mid-latitude troposphere, with a zonally-connected jet and its attendant eddies (e.g. Rintoul et al., 2002, 2004). This is because in the latitude range of Drake Passage, there are no continuous meridional barriers. So there can be no net meridional transport in the region, and that transport must be carried by eddies. Eddies thus transport buoyancy across the Antarctic Circumpolar Current (ACC) as storms transport heat across the Jet Stream. The dynamics of the ACC are therefore believed to be fully nonlinear.

In contrast are the subtropical gyres, where meridional barriers permit a Sverdrup balance in the ocean interior. Observations suggest that such a balance exists, within the errors, in the upper water column in the North Atlantic (Leetmaa et al., 1977; Wunsch and Roemmich, 1985) and North Pacific (Hautala et al., 1994). This favors the use of *linear models* of the wind-driven circulation, as in the seminal works of Stommel (1948) and Munk (1950). These models, with their frictional western boundary currents, yield circulations which broadly resemble those observed (Godfrey, 1989; Vallis, 2006).

This is not to say that eddies are not important here. They are likely instrumental in phenomena like the , recirculation gyres (e.g. Jayne and Hogg, 1999). Indeed, adding nonlinearity to the Stommel and Munk models produces recirculations (Bryan, 1963; Veronis, 1966). They may also be important in setting the vertical structure of the wind-driven circulation, something which is simply specified in the linear models. Nevertheless these models provide a plausible zeroth-order description of the large scale flow and are still used as testbeds for various processes.

No linear model of the Southern Ocean has been similarly accepted. This is not however for lack of linear models. But the existing models differ widely in their dynamics and predicted transports. This may explain in part why there is still widespread disagreement about the fundamental dynamics. It remains uncertain for instance whether the ACC transport is determined by the wind stress, its curl or by thermohaline forcing (e.g. Gnanadesikan and Hallberg, 2000).

These linear models are the subject of the present review. Because they are generally overlooked, many readers may even be unfamiliar with them. Thus we will revisit them, and study in particular how they are dynamically related. In addition, we wish to see to what extent the models resemble observations, both from in situ data and from GCMs. Some of the models display a surprising degree of realistic structure, and are perhaps worthy of further study.

1.1. The models

Fundamentally, the linear models differ in how they treat the *geostrophic contours* in the Southern Ocean. The geostrophic contours represent the stationary portion of the potential vorticity, e.g. that due to the Coriolis effect. Some of the models have contours *blocked* by lateral barriers while others have *closed* contours which reconnect globally. With weak friction, wind-driven models with blocked contours exhibit a Sverdrup interior and western boundary currents. But the Sverdrup balance fails with closed contours because there can be no net cross-contour flow (there are no western boundary currents in which the cross-contour flow can return). Thus another agent, like bottom friction, must balance the wind stress. With weak friction, the flow is mainly along the geostrophic contours and can be very strong (Welander, 1968; Greenspan, 1968; Young, 1981; Isachsen et al., 2003).

Stommel (1957) contended that the geostrophic contours are blocked in the Southern Ocean. The Scotian Island Arc spans the latitude range to the east of the Drake Passage and presents an obstacle to any throughflow. Stommel suggested the arc could act as a "porous" western boundary, permitting the ACC to pass through and feed the Falkland Current. Then the interior would be in Sverdrup balance and, Stommel conjectured, the ACC's transport could be determined from integrating the wind stress curl, as in a subtropical gyre. Subsequent tests of this, derived from a circumpolar integral of the curl around the globe at the latitude of the tip of South America, yielded estimates comparable to transports measured in Drake Passage (Baker, 1982; Godfrey, 1989; Chelton et al., 1990; Warren et al., 1996).

However, Stommel did not derive an analytical model to support his idea. But Ishida (1994) considered a model which was dynamically equivalent (Section 3). The model employs a flat-bottomed channel, where the geostrophic contours (latitude lines) are blocked at all latitudes by two disconnected meridional barriers. The solution has a Sverdrup interior, but also exhibits a piecewise zonal, circumpolar jet. The latter occurs because the meridional barriers are disconnected, so that pressure differences can exist between them. In this model, the strength of the circumpolar flow is not determined by an integral of the wind stress curl but of the stress itself. Webb (1993), who examined a similar model independently, suggested it could also account for the splitting of the ACC into branches, if additional barriers (representing, for example, the Kerguelen Plateau) were introduced.

The other possibility is that Drake Passage is not blocked and that the geostrophic contours are closed. Gill (1968) examined such a case, using a channel blocked by a barrier in the northern half-domain and open in the southern half (Section 4). In the north, the flow is approximately in Sverdrup balance, but in the south the balance is between the transport in the surface and bottom Ekman layers. This model produces transports which are much larger than observed, unless one uses fairly large bottom drag coefficients.

Many believe that Gill's model fails because it lacks bottom topography. Munk and Palmen (1951) suggested that the wind stress could be balanced by pressure gradients across bottom topography rather than by bottom friction. Support for this *form drag balance* has been found in numerous modelling studies (e.g. Treguier and McWilliams, 1990; Stevens and Ivchenko, 1997; Gille, 1997; Gnanadesikan and Hallberg, 2000; Gent et al., 2001). However, the form drag does not predict the transport of the ACC. In fact, it is equivalent to a mass conservation statement, in which the surface Ekman transport is balanced by geostrophic flow between topographic features (Warren et al., 1996; Section 7.1). Thus

Please cite this article in press as: LaCasce, J.H., Isachsen, P.E. The linear models of the ACC. Prog. Oceanogr. (2010), doi:10.1016/j.pocean.2009.11.002

the form drag balance may apply instead to the meridionally overturning circulation, which may or may not be related to the ACC.

The first to incorporate topography in an analytical model of the ACC was Kamenkovich (1962) (see also Johnson and Hill, 1975). His solution involved a novel integration along the geostrophic contours (which are just the contours of f/H in a barotropic fluid; Section 2). With weak bottom drag, the flow is primarily along these contours. However, f/H is rather convoluted in the Southern Ocean, with large closed gyres. So the solution does not resemble the actual ACC, and has only a weak circumpolar component (Krupitsky et al., 1996).

This suggests that topography is too dominant in a barotropic model. Stratification weakens topographic steering, as the bottom velocities are usually weaker than the depth-averaged velocities. Killworth (1992) found that the ACC in the FRAM simulation of the Southern Ocean (FRAM Group, 1991) exhibited an *equivalent barotropic* structure, so that the bottom velocities were parallel to, but weaker than, the surface velocities. Krupitsky et al. (1996) exploited this in a model (Section 5) similar to Kamenkovich's. But because the model is equivalent barotropic, the geostrophic contours are given by $f/F(H)$, where $F(H)$ is a filtered function of the topography (see also Marshall, 1995; Killworth and Hughes, 2002). The authors obtained solutions whose structure and transport were similar to those in the FRAM model (Krupitsky et al., 1996; Ivchenko et al., 1999).

Hereafter we consider how these are dynamically related. We focus especially on two models, those of Ishida (1994) and Krupitsky et al. (1996). The latter exhibits structure very like that of the actual ACC (Section 6). The former captures the essential dynamics of the latter in the relevant parameter range, and suggests a way in which the circumpolar transport can be estimated analytically. We identify too which aspects of the circulation the models fail to explain.

2. Equations

The models considered hereafter assume either a barotropic or equivalent barotropic vertical structure. The barotropic assumption is familiar, that there is no vertical shear. The equivalent barotropic construct is less familiar in the oceanic literature but is well-known in the atmospheric context, having been developed for weather forecasting during the 1940s and 1950s (Charney, 1949; Fjørtoft, 1952; Carlson, 1991). The construct permits stratification, but the thermal wind is everywhere parallel to the geostrophic velocities at the surface. So while the magnitude of the velocity varies with depth, its direction does not. Under this assumption, the density field is passive and one solves only for the velocities.

We will derive equations for the equivalent barotropic case; the barotropic case can then be recovered by setting the vertical shear to zero. The key assumption is that the vertical structure is separable:

$$\vec{u}(x,y,z,t) = \vec{u}_s(x,y,t)P(z) \tag{1}$$

and

$$p(x,y,z,t) = p_s(x,y,t)P(z) \tag{2}$$

where $\vec{u}$ and p are the horizontal velocities and the dynamic pressure and $\vec{u}_s$ and p_s are corresponding values at the surface. Substituting these into the horizontal momentum equations yields:

$$P\frac{\partial}{\partial t}\vec{u}_s + P^2\vec{u}_s\cdot\nabla\vec{u}_s + f\hat{k}\times P\vec{u}_s = -\frac{1}{\rho_0}P\nabla p_s + \frac{\partial}{\partial z}\frac{\vec{\tau}}{\rho_0} + \nu P\nabla^2 u_s \tag{3}$$

where $\vec{\tau}$ is the applied stress (e.g. Gill, 1982). We assume the motion is steady and linear and neglect the first two terms. Integrating in the vertical yields:

$$f\hat{k}\times F\vec{u}_s = -\frac{1}{\rho_0}F\nabla p_s + \frac{\vec{\tau}_w}{\rho} - RP(-H)\vec{u}_s + \nu F\nabla^2\vec{u}_s \tag{4}$$

Here τ_w is the wind stress, R is a linear bottom friction coefficient and

$$F(x,y) \equiv \int_{-H}^{0} P(z)dz \tag{5}$$

is the integral of the vertical structure function, $P(z)$. Note that if the flow is barotropic,

$$P(z) = 1 \tag{6}$$

and

$$F(x,y) = H(x,y) \tag{7}$$

Then Eq. (4) reduces to the steady, linear shallow water momentum equation.

The continuity equation, under the Boussinesq approximation, is:

$$\frac{\partial}{\partial x}u + \frac{\partial}{\partial y}v + \frac{\partial}{\partial z}w = 0 \tag{8}$$

Substituting in (1), integrating in the vertical and rearranging yields:

$$\frac{\partial}{\partial x}(Fu_s) + \frac{\partial}{\partial y}(Fv_s) = 0 \tag{9}$$

As with the momentum equation, the shallow water continuity equation is recovered if $F = H$. The continuity equation allows the definition of a transport streamfunction:

$$Fu_s = -\frac{\partial}{\partial y}\psi, \quad Fv_s = \frac{\partial}{\partial x}\psi \tag{10}$$

Dividing the momentum Eq. (4) by F, taking the curl and invoking the streamfunction yields a potential vorticity equation:

$$J\left(\psi, \frac{f}{F}\right) = \nabla\times\frac{\vec{\tau}}{\rho F} - R\nabla\cdot\left[\frac{P(-H)}{F^2}\nabla\psi\right] + \nu\nabla^2\left(\frac{\partial}{\partial x}\frac{1}{F}\frac{\partial\psi}{\partial x} + \frac{\partial}{\partial y}\frac{1}{F}\frac{\partial\psi}{\partial y}\right) \tag{11}$$

where $J(a,b)$ is the Jacobian function. Eq. (11) states that flow across contours of f/F, which are the geostrophic contours in the equivalent barotropic system, can only occur in response to wind forcing or friction. Without such forcing, the flow is everywhere parallel to f/F. Minus the lateral friction, this is the equation used by Krupitsky et al. (1996) and Ivchenko et al. (1999) in their studies with the equivalent barotropic model (Section 5).

If the flow is barotropic, so that $F = H$, Eq. (11) reduces to the steady, linear shallow water vorticity equation:

$$J\left(\psi, \frac{f}{H}\right) = \nabla\times\frac{\vec{\tau}}{\rho H} - R\nabla\cdot\left[\frac{1}{H^2}\nabla\psi\right] + \nu\nabla^2\left(\frac{\partial}{\partial x}\frac{1}{H}\frac{\partial\psi}{\partial x} + \frac{\partial}{\partial y}\frac{1}{H}\frac{\partial\psi}{\partial y}\right) \tag{12}$$

Then the geostrophic contours are given by f/H. This is the equation considered by Kamenkovich (1962). If, in addition, the bottom is flat and we invoke the β-plane approximation, $f = f_0 + \beta y$, we have:

$$\beta\frac{\partial}{\partial x}\psi = \frac{1}{\rho}\nabla\times\vec{\tau} - r\nabla^2\psi + \nu\nabla^4\psi \tag{13}$$

where $r = R/H$. Now the geostrophic contours are latitude lines. Excluding lateral friction, this is the vorticity equation used by Gill (1968; Section 4) and Ishida (1994; Section 3). It is also the basis of Stommel's (1948) model of the Gulf Stream. Thus Eq. (11) encompasses *all* the linear models discussed in the present article.

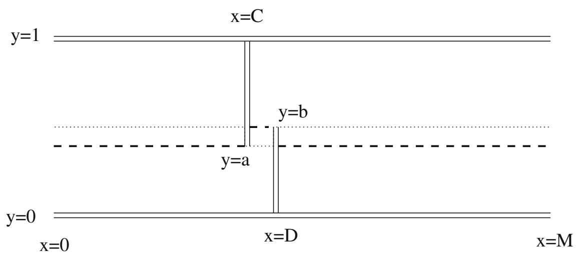

Fig. 1. The channel geometry of Ishida's model. The thick dashed curve indicates the position of the zonal boundary layers, while the dotted lines show the contour used for the island rule integral.

Hereafter we examine these models. We begin with the barotropic, flat bottom cases, before proceeding to the equivalent barotropic model with topography.

3. Ishida's model

Though not the first of the linear models, Ishida's (1994) model exhibits many features found in the more complicated models. A similar model was examined independently by Webb (1993) (see also Hughes, 2002).[1] As noted, this model most closely represents the one envisioned by Stommel (1957). In this, the Southern Ocean is a channel with two meridional barriers (Fig. 1). The northern barrier represents South America and the southern one represents the Antarctic peninsula/Scotian Island Arc. The channel is periodic, so that $\psi(M,y) = \psi(0,y)$.

The model employs Eq. (13) without lateral friction. It is useful to non-dimensionalize the equation, thus:

$$\frac{\partial}{\partial x}\psi = \mathscr{T}\nabla \times \vec{\tau} - \delta\nabla^2\psi \qquad (14)$$

where

$$\delta \equiv \frac{r}{\beta L}, \quad \mathscr{T} = \frac{T}{\rho\beta HUL}$$

Here T is the amplitude of the wind stress, L the N–S extent of the channel and U the velocity scale. Thus bottom friction is weak if $\delta \ll 1$. Then frictional dissipation is confined to boundary layers and the vorticity equation in the interior is approximated by the Sverdrup relation:

$$\frac{\partial}{\partial x}\psi = \nabla \times \vec{\tau} \qquad (15)$$

The parameter $\mathscr{T}$ is thus of order unity, implying the velocities scale as $U \approx T/(\rho\beta HL)$.

The streamfunction at a given latitude is found by integrating (15) west from the nearest eastern boundary.[2] The integral is particularly simple if the wind stress is only a function of y:

$$\psi(x) = \psi_E - \frac{\partial\tau^x}{\partial y}(x - x_E) \qquad (16)$$

where x_E is the position of the nearest eastern boundary and ψ_E is the value of the streamfunction on that boundary. We can set $\psi_E = 0$ on the northern barrier, without loss of generality. But we cannot assume $\psi_E = 0$ on the southern boundary because the two barriers are disconnected. Rather, we set $\psi_E = \Gamma$, where Γ is a constant. This is equal to the transport between the barriers, as follows from integrating the meridional velocity across the gap between the barriers:

$$\int_C^D Hv dx = \int_C^D \frac{\partial}{\partial x}\psi dx = \psi(D) - \psi(C) = \Gamma \qquad (17)$$

Thus Γ is the strength of the model's circumpolar flow.

Friction acts in boundary layers, of which there are two types. First, there are Stommel layers on the eastern sides of the meridional boundaries (Fig. 1). These decay to the east as $exp(-x/\delta)$ and act to reset the streamfunction to the value on the barrier. There are also boundary layers in the interior. These smooth discontinuities in the Sverdrup streamfunction which occur because the northern and southern barriers are on different meridians. Consider the streamfunction just west of the southern tip of the northern barrier. To the south of the line $y = a$, the streamfunction, from (16), is:

$$\psi(x, a^-) = \Gamma - \frac{\partial\tau^x}{\partial y}(a)(x - D) \qquad (18)$$

But north of $y = a$, the streamfunction is:

$$\psi(x, a^+) = -\frac{\partial\tau^x}{\partial y}(a)(x - C) \qquad (19)$$

So there is a discontinuity in the streamfunction along the line $y = a$:

$$\triangle\psi(x, a) = \frac{\partial\tau^x}{\partial y}(a)(D - C) - \Gamma \qquad (20)$$

Without friction, this jump would produce a zonal jet with an infinite velocity. But friction smooths the jump, reducing the velocities. These interior boundary layers, centered on the dashed lines in Fig. 1, are regions of strong zonal flow. This is the circumpolar current in the Ishida model. The boundary layers spread toward the west, as in a diffusive layer, with a thickness proportional to $\delta^{1/2}$ (Appendix A).

There remains one unknown: the circumpolar transport, Γ. This can be found via an integral relation, equivalent to Godfrey's (1989) island rule.[3] This derives from the non-dimensionalized momentum equation, which can be written:

$$\hat{f}\hat{k} \times \vec{u} = -\mathscr{P}\nabla p + \vec{\tau} - \delta\vec{u} \qquad (21)$$

where

$$\hat{f} = \frac{f(y)}{\beta L}, \quad \mathscr{P} = \frac{P}{\rho\beta UL^2}$$

We assume that $f_0 \approx \beta L$, for consistency with the scaling of the vorticity equation. Integrated around a closed circuit, this is:

$$\oint \hat{f}\vec{u} \cdot \hat{n}dl = \oint \vec{\tau} \cdot dl - \delta \oint \vec{u} \cdot dl \qquad (22)$$

The circuit is indicated by the dotted lines in Fig. 1. It is zonal in the interior and meridional along the eastern boundaries. We choose this particular path because bottom friction is assumed to be negligible along the eastern boundaries. As there is no flow into the boundaries and as the wind is zonal, the meridional segments do not contribute to the integral. The full integral is given in Appendix A.

Three representative solutions, with different values of the bottom friction coefficient, δ, are shown in Fig. 2. We use a sinusoidal wind stress, given by:

[1] Webb (1993) examined a model with a geometry like that of Ishida (1994), but forced by sources and sinks of fluid rather than a wind stress. Hughes (2002) generalized Webb's model to include stratification and bottom topography, and discussed it in relation to Stommel's (1957) conjectured circulation.

[2] This follows from the presumption of western boundary layers. Interestingly, Stommel, 1957 suggested a possible *eastern* boundary current west of the Antarctic Peninsula. Hughes, 2002 explored the consequences of such a layer. But eastern boundary layers are not possible with only bottom friction (Stommel, 1948; Pedlosky, 1987).

[3] A similar relation is employed by Kamenkovich (1962).

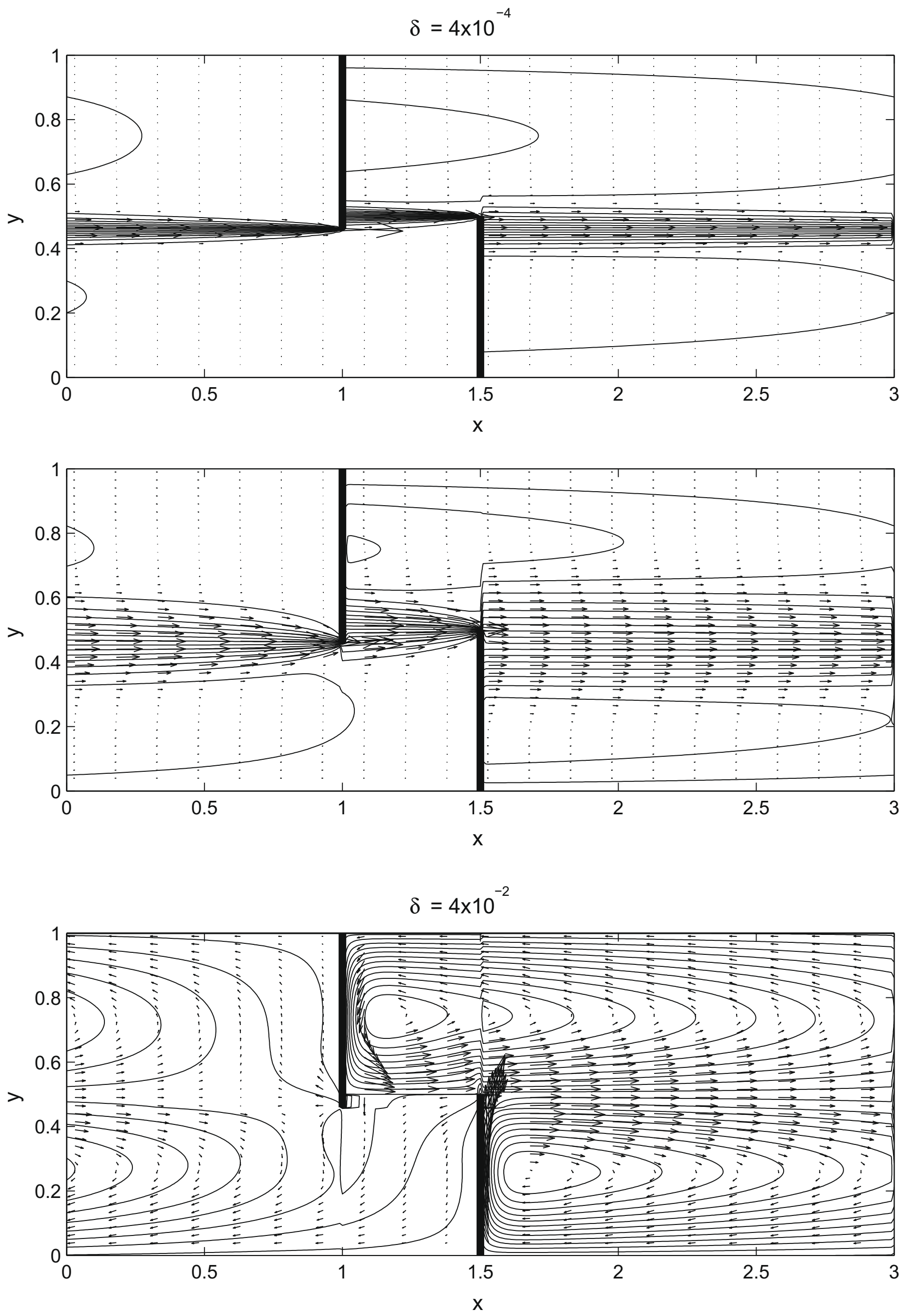

Fig. 2. The Ishida model solution with three values of the non-dimensional bottom friction coefficient, δ.

$$\vec{\tau} = \tau^x \hat{i} = \frac{1}{2}[1 - cos(2\pi y)]\hat{i} \tag{23}$$

(recall that the scaled N–S extent of the channel is one). The solution with the weakest damping ($\delta = 4 \times 10^{-4}$, upper panel) exhibits two gyres, with counter-clockwise flow in the north and clockwise flow in the south. Between the barriers is a jet, which flows eastward. The jet is zonal except where it passes though western boundary layers on the eastern sides of the barriers. The jet coincides with the interior boundary layers discussed above, and its narrowing from west to east reflects the westward spreading of those layers.

The solution with $\delta = 4 \times 10^{-3}$ (middle panel) is similar, except that the jet is wider and weaker. Note there is a mismatch in the jets north of the southern barrier (the jet suddenly narrows). Ishida (1994) suggested the bottom friction should be weak enough so that the meridional spreading to the east of the barrier does not cross the northern tip, precisely to avoid this. The model can be modified to smooth the transition, by including a boundary layer at the barrier tip (e.g. Gill, 1968). But this complicates the solution and does not affect the transport.

The solution with $\delta = 4 \times 10^{-2}$ (lower panel) has essentially no circumpolar flow at all. The solution is instead dominated by the two gyres. Note that these gyres are not stronger than in the previous two cases (being independent of bottom drag); they only appear stronger because the jet is absent.

Shown in Fig. 3 is the jet transport as a function of bottom friction from a suite of such solutions. The transport and friction have been dimensionalized, for comparison with subsequent numerical solutions. In particular, we plot $\Gamma_{dim} = \Gamma T(\rho\beta)^{-1}$ against $R = \beta H L \delta$.

Please cite this article in press as: LaCasce, J.H., Isachsen, P.E. The linear models of the ACC. Prog. Oceanogr. (2010), doi:10.1016/j.pocean.2009.11.002

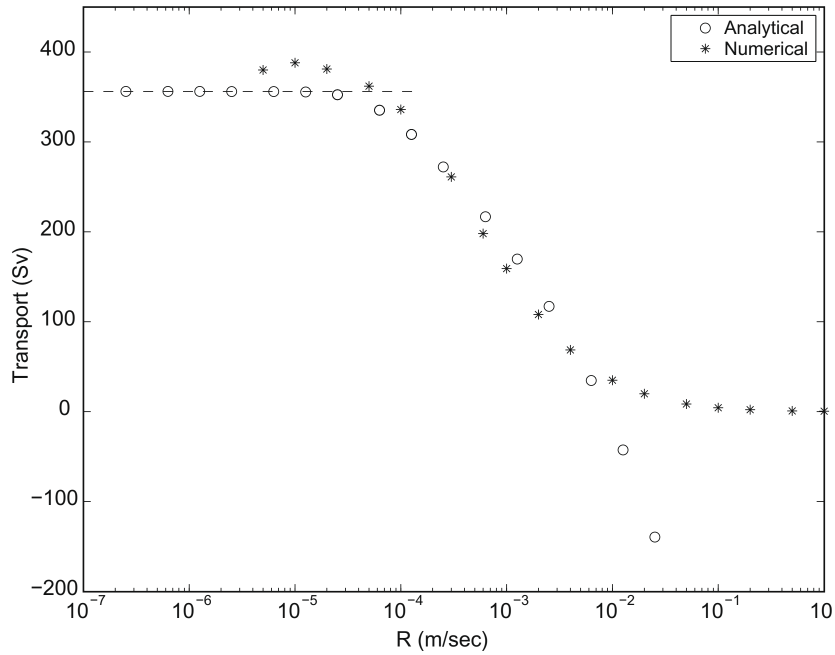

Fig. 3. The jet transport as a function of bottom friction for the Ishida model and for a numerical solution in a similar channel. The transport and friction for the analytical model have been dimensionalized, such that $\Gamma_{dim} = \Gamma T(\rho\beta)^{-1}$ and $R = \beta HL\delta$. The dashed line indicates the inviscid estimate for the analytical solution, in which friction is ignored in the island integral.

We see that the transport asymptotes to a constant value for small drag coefficients and decreases monotonically with stronger damping. The asymptotic limit (roughly 350 Sv) is substantially larger than in the ACC, but the model has not been "tuned" in any way. Note too that the transport becomes *negative* at the largest values of R.

This dependence can be understood as follows. The extent to which friction enters the island integral depends on how much the jet (centered on the dashed lines in Fig. 1) overlaps the island contour (the dotted lines). With vanishing friction there is no overlap, so that the surface Ekman transport is balanced entirely by the meridional flow. Then the (non-dimensional) transport is given by:

$$\Gamma = \frac{M\tau(b) + (C - D)[\tau(b) - \tau(a)]}{\hat{f}(b) - \hat{f}(a)} \tag{24}$$

The corresponding dimensional value is indicated by the dashed line in Fig. 3.

With larger values of R, the jet overlaps the Island curve and friction enters the Island integral. Thus the bottom Ekman layer partially balances the surface Ekman transport, and the circumpolar transport is reduced. If R is large enough the jet actually reverses, so that the surface and bottom Ekman transports are both to the north.

As discussed by Ishida (1994), the transport, Γ, depends on the positions and extent of the barriers. The dependence on the separation in x is relatively weak. From (24), the transport is approximately linearly proportional to the barriers' meridional separation, as long as the wind stress at the latitudes of the barrier tips is different ($\tau(b) \neq \tau(a)$). In our example those winds are equal, so there is no dependence at all on the meridional separation.

On the other hand, the transport is inversely proportional to the latitudinal overlap between the barriers. As the overlap goes to zero, the transport becomes infinite. Then the island contour becomes zonal and the meridional transport term drops out. If the overlap is increased, the transport decreases. So a more realistic asymptotic transport in Fig. 1 can be had by simply increasing the overlap.

Increasing the overlap has another interesting effect: it increases the distance between the island contour and the jet axis. So with the same value of R, bottom friction is *less* important for the circumpolar transport with a large overlap than with a small one.

3.1. Numerical solutions

We can test the analytical solutions by computing comparable numerical solutions employing the same channel geometry. For these solutions, we used the Regional Oceanic Modeling System (ROMS; Shchepetkin and McWiliams, 2005). The model was configured for a channel, 9000 km in length and 3000 km wide, and centered at 60S. We ran the model without advection, in the barotropic mode. We used a linear bottom drag, as in the analytical model, and used no explicit diffusion of momentum. We used the same wind stress as in (23), with an amplitude of 0.1 N/m^2, and ran the model to a steady state. Note that the model solves the horizontal momentum and continuity equations, rather than the vorticity equation in (13).

The sea surface height (SSH) fields obtained from three such runs are shown in Fig. 4. The solution in the upper panel had a bottom friction coefficient, R, of 10^{-4} m/s (yielding the same value of δ used for the upper panel of Fig. 2). As with the analytical solution, there are gyres in the north and south separated by a piecewise zonal jet, with the latter spreading to the west from the barrier tips. The oscillations emanating from the eastern sides of the barriers are reflected Rossby waves, initiated during spin-up and not yet dissipated away by the bottom drag.

The solution with intermediate friction ($R = 10^{-3}$ m/s, middle panel) also resembles its analytical counterpart (Fig. 2). The westward spreading is evident and the jet is wider. Note too that the flow north of the tip of the southern boundary smoothly joins the flow to the west.

However, the run with the strongest bottom drag ($R = 10^{-2}$ m/s, bottom panel) differs from its analytical counterpart. In particular, the numerical solution reveals a jet where the analytical model had little circumpolar flow at all (Fig. 2). The jet

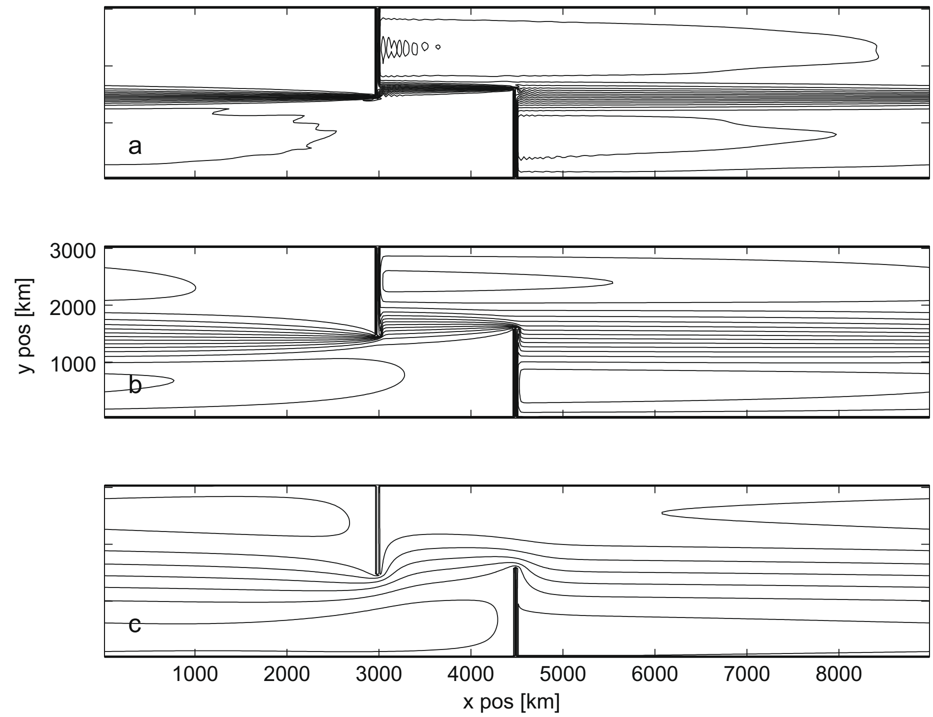

Fig. 4. The SSH fields from three solutions with ROMS, with $R = 10^{-4}$ m/s (top), $R = 10^{-3}$ m/s (middle) and $R = 10^{-2}$ m/s (bottom).

is much less zonal than in the cases with weaker damping, exhibiting smooth north–south deviations around the barriers.

The transport from a number of such runs is plotted in Fig. 3. These estimates derive from averaging the transport in Drake Passage over the final third of each run. In the weak friction limit, the transport asymptotes to a value somewhat greater than 350 Sv, the asymptotic limit in the analytical solution (the slight difference is due to small differences in the barrier lengths in the models). As in the analytical model, the transport decreases with increasing friction; but here the transport goes to zero with large friction rather than becoming negative.

This reason for the latter difference can be inferred from Fig. 5. This shows the three terms in the vorticity balance (13) evaluated in the model along the latitude line at y = 2000 km (north of the jet axis, in the northern gyre). With $R = 10^{-4}$ m/s, the βv term approximately balances the wind stress curl over much of the interior; only in the western boundary layer is bottom friction important. With $R = 10^{-3}$ m/s, all three terms are important in the interior, implying the Sverdrup balance no longer holds in the interior. With $R = 10^{-2}$ m/s, βv is *unimportant* and the bottom Ekman layer is the primary agent balancing the wind. Thus the analytical model, which assumes a Sverdrup interior for all values of the bottom friction, differs in this limit.

Friction plays an interesting role in these models. It is unimportant *in the gyres* in the analytical model, which has a Sverdrup interior. But it can be important for the circumpolar transport, if the jet overlaps the island contour. Thus friction can be important for the ACC, despite that it isn't for the gyres. The numerical solutions suggest friction acts in the gyres as well, with larger bottom drag coefficients. But in the limit of vanishing bottom friction, both the analytical and numerical models have gyres and jets whose strengths are *independent of bottom drag*.

4. Gill's model

If we remove the southern barrier, we have Gill's (1968) model. Now the latitude lines are blocked only in the northern half of the domain. The solution in the north derives from the integrated Sverdrup relation (15),[4] as in Ishida's model. The solution in the south differs, because the Sverdrup balance no longer holds. Instead, the solution is determined by the zonally-integrated x-momentum equation:

$$\oint \tau^x dx = \delta \oint u dx = -\delta \oint \frac{\partial \psi}{\partial y} dx \tag{25}$$

Note this is just the island rule (22), integrated along a latitude line.

With a wind stress which varies only with latitude the solution is, to first order:

$$\psi(y) = \Gamma - \frac{1}{\delta} \int_0^y \tau^x dy \tag{26}$$

The full solution is complicated and we will not reproduce it here. Instead, we use the ROMS model to derive a numerical solution for the problem, employing the same geometry as with the Ishida calculation but without the southern barrier. The result, with a bottom friction coefficient of $R = 10^{-4}$ m/s, is shown in Fig. 6. The flow is dominated by an essentially zonal flow, intensified in the southern half of the domain. This overshadows the solution in the north, which is dynamically similar to that in the Ishida model, with a Sverdrup gyre and a western boundary current on the eastern side of northern barrier. We see only that some of the streamlines appear to intersect the boundary.

Of central interest here is the total transport, Γ. Assuming the channel streamfunction vanishes at $y = a$ and using the wind stress in (23), this is:

$$\Gamma = \frac{1}{\delta} \int_0^a \tau(y) dy = \frac{1}{2\delta} \left[a - \frac{1}{2\pi} \sin(2\pi a) \right] \tag{27}$$

[4] Gill (1968) allowed for the possibility that bottom friction modifies the solution over the whole domain. In his formulation, the Sverdrup balance is the lowest order balance in the northern interior.

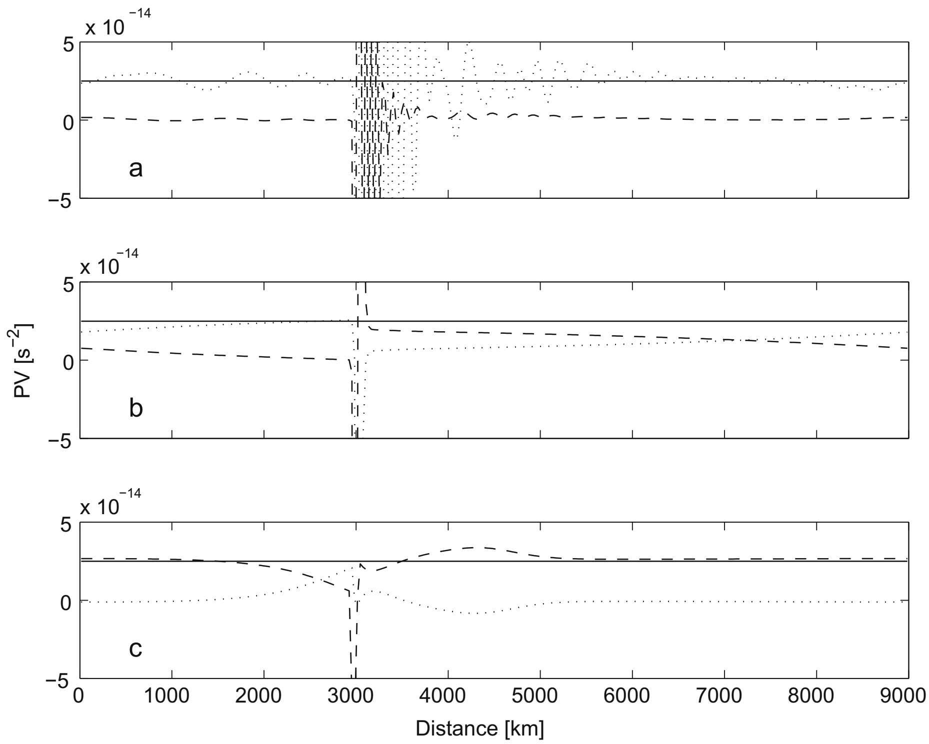

Fig. 5. The terms in the vorticity equation at $y = 2000$ km vs. x, from the three simulations shown in Fig. 4. The βv term is represented by the dotted line, the (constant) wind stress curl by the solid line and the bottom stress term by the dashed line. The oscillations in the western boundary layer in the upper panel come from short Rossby waves.

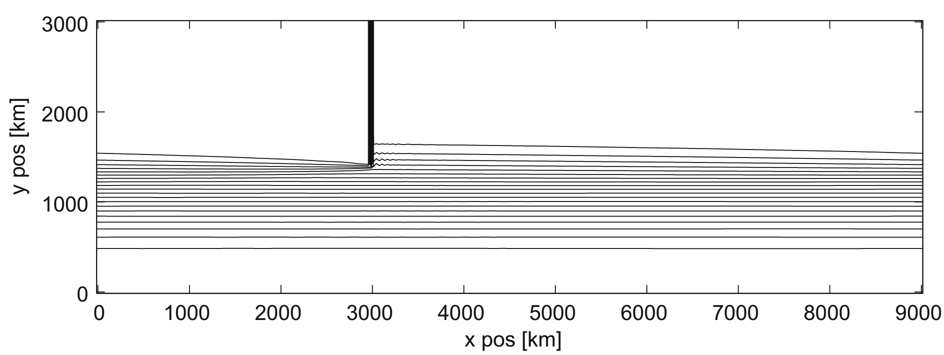

Fig. 6. The SSH from a ROMS calculation using the Gill geometry, with $R = 10^{-4}$ m/s.

The corresponding dimensional transport is:

$$\Gamma = \frac{H\tau_0}{\rho R}\left[a - \frac{L}{2\pi}sin\left(\frac{2\pi a}{L}\right)\right] \quad (28)$$

So the transport is inversely proportional to the bottom friction. Instead of asymptoting to a constant value, as in Ishida's model (Fig. 3), the transport in the Gill model increases without bound as $R \to 0$. Using the channel dimensions and the wind stress amplitude (0.1 N/m^2) from the numerical example, the transport is $0.3/R$ Sv. With $R = 10^{-4}$ m/s, this yields 3000 Sv. The same transport is found integrating across the southern half of the domain in the numerical solution, after the latter equilibrates.

The large transport is a familiar problem with the Gill model: reasonable values of the transport require larger values of bottom friction. To obtain a transport like that in Drake Passage requires a friction coefficient which is 20 times larger. Next we explore the extent to which topography alters the picture.

5. Equivalent barotropic model with topography

As noted earlier, the justification for using such a model comes from Killworth (1992), who found that the ACC in the FRAM model had an equivalent barotropic structure. Sun and Watts (2001) found a similar vertical structure in their analysis of hydrography from the Southern Ocean, as did Killworth and Hughes (2002) with data from a simulation with the OCCAM model (Saunders et al., 1999). The equivalent barotropic (EB) model was first applied to the Southern Ocean by Krupitsky et al. (1996) and was compared to fields from the FRAM simulation by Ivchenko et al. (1999).

In this model, the geostrophic contours are determined by f/F, where F is given in (30). These contours are intermediate between latitude lines and f/H contours, depending on the vertical structure function, $P(z)$. To see this, consider that $P(z)$ is an exponential function:

$$P(z) = exp\left(\frac{z}{z_0}\right) \quad (29)$$

Please cite this article in press as: LaCasce, J.H., Isachsen, P.E. The linear models of the ACC. Prog. Oceanogr. (2010), doi:10.1016/j.pocean.2009.11.002

Killworth (1992) deduced an exponential profile from the FRAM data and an exponential was also used by Krupitsky et al. (1996) and Ivchenko et al. (1999). With this, we have:

$$F = \int_{-H}^{0} Pdz = z_0\left[1 - exp\left(-\frac{H}{z_0}\right)\right] \tag{30}$$

In deep water, where $H \gg z_0$:

$$F \approx z_0$$

So the geostrophic contours, f/F, are like latitude lines. In shallow water, where $H \ll z_0$:

$$F \approx H$$

So the contours revert to f/H. Thus f/F effectively filters out deep topography from the geostrophic contours.

A second point with the EB model is that the bottom drag depends on $P(-H)$, from (11). With the exponential profile above, $P(-H)$ is vanishingly small when $H \gg z_0$; so the drag is weak in deep water. Krupitsky et al. (1996) and Ivchenko et al. (1999) included an additive constant to their exponential profiles, presumably to avoid this effect. But we will not do so, to reduce the number of free parameters.

To calculate solutions, we again use the ROMS model, which we modified to solve the equivalent barotropic momentum and continuity Eqs. (4) and (9). As before, we ran the model to a steady state with a constant wind stress, using various e-folding scales, z_0. Note that Krupitsky et al. (1996) calculated numerical solutions to (11) directly, but our spin-up calculations produce consistent results.

The model resolution was 1° by 0.5°, on a spherical grid, and we again used no momentum advection or diffusion. For the wind stress, we used the Hellerman and Rosenstein (1983) climatology. We also tested the Trenberth et al. (1989) and Southampton SOC GASC97 (Josey et al., 1999) climatologies and obtained qualitatively similar results. For topography, we used a 1° data set (from the National Geophysical Data Center), smoothed once with a nine-point filter. Thus we do not resolve topographic scales less than roughly 100 km.

Shown in the upper panel of Fig. 7 is the sea surface height from a solution with an e-folding scale of $z_0 = 500$ m. We used a small bottom drag coefficient, $R = 10^{-5}$ m/s. Because of this, wave-like oscillations are present throughout the simulation. A gyre is evident in the northern part of the domain, but the flow is otherwise dominated by a nearly zonal jet in the Drake Passage latitudes. Significantly, this run *never equilibrated*; the transport increased until the simulation became numerically unstable. At the time shown, the circumpolar transport was 1100 Sv and the difference in sea surface height across the stream was on the order of 20 m!

The large transport can be traced back to the f/F contours, which are nearly zonal and unblocked in the Drake Passage latitudes (lower panel of Fig. 7). In line with Gill's model, we expect that the Sverdrup balance does not apply here and that the primary balance is between the wind stress and bottom drag. However, the drag is very weak because the depth greatly exceeds z_0. So the wind forcing is essentially unbalanced. Had we used an additive constant in $P(z)$, as Krupitsky et al. (1996) did, this would not happen, but the jet would still be zonal and the transport large.

Increasing z_0 to 800 m yields the SSH field in the upper panel of Fig. 8. Unlike the previous example, this run does equilibrate. Note again that there are waves which have not yet dissipated, due to the weak bottom drag. The flow in the Drake Passage latitudes is still strong, but a portion of the current peels off to the north, moving along the South American coast and crossing to the Kerguelen Plateau (at 80E). The current then proceeds southward, east of the plateau, to rejoin the southern branch. However the transport in Drake Passage, 755 Sv, is still fairly large and the height difference on the order of 10 m.

The f/F contours for this case are shown in the lower panel of Fig. 8. The primary difference is that with $z_0 = 800$ m, the Kerguelen Plateau exerts a greater influence on *f*/*F*. It blocks most of the Drake Passage latitudes, preventing the zonal jet seen with $z_0 = 500$ m.

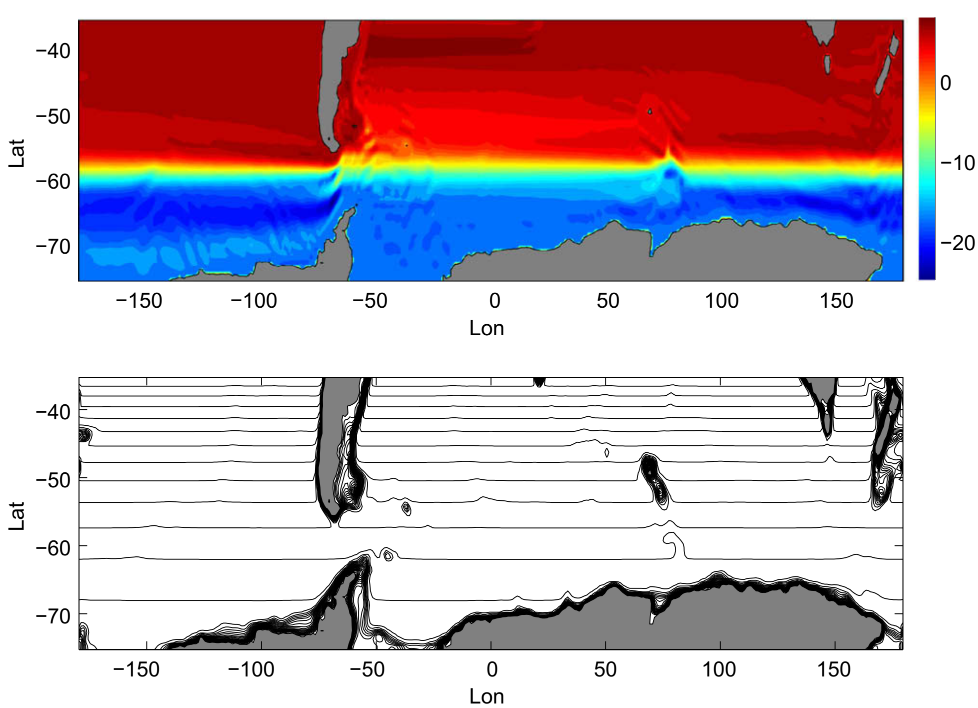

Fig. 7. The sea surface height (in m) from a solution with $z_0 = 500$ m and $R = 10^{-5}$ m/s. The blue shades reflect low SSH values while the red are high. The field shown occurs during spin-up, as this run does not equilibrate. The lower panel shows the corresponding f/F contours. (For interpretation of the references to colour in this figure legend, the reader is referred to the web version of this article.)

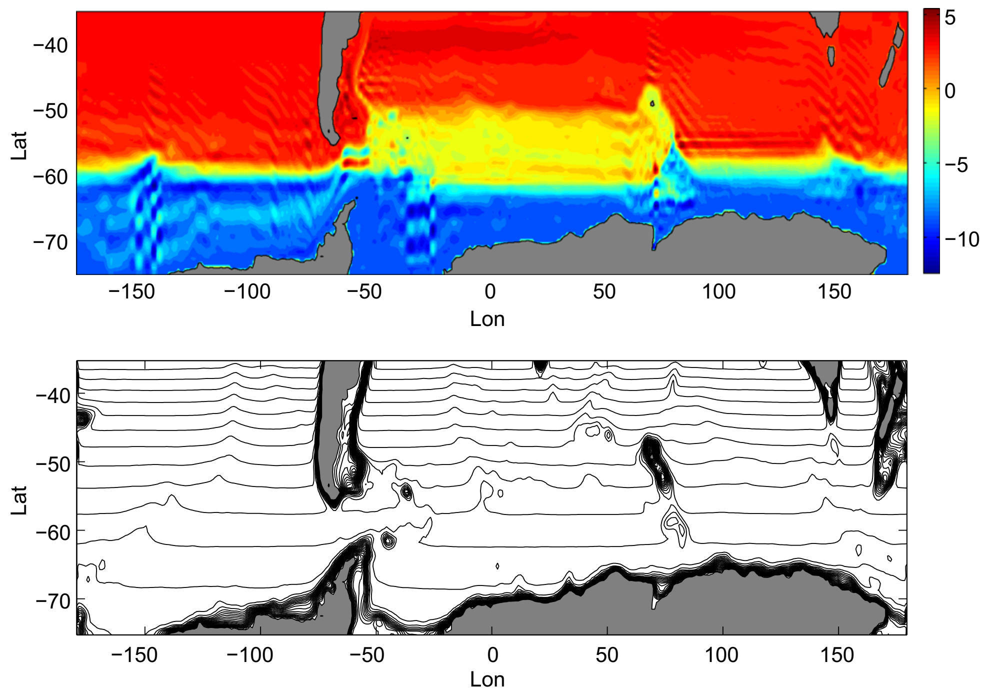

Fig. 8. Sea surface height from an equilibrated simulation with $z_0 = 800$ m and $R = 10^{-5}$ m/s.

We can capture the essential elements of this solution with a modified version of Ishida's model (Fig. 9). The two barriers at left no longer overlap, leaving the "Drake Passage" open. However, the latitude lines are blocked by a "Kerguelen" Island to the east. With this configuration, there are two unknowns: the streamfunction on Antarctica and that on the island. This requires two island contours, as indicated by the dashed and dash-dotted lines in the figure. The solution with friction is not trivial, but the inviscid solution is straightforward, involving a pair of coupled equations:

$$\begin{pmatrix} f_k - f_g & 0 \\ f_j - f_h & f_h - f_j \end{pmatrix} \begin{pmatrix} \Lambda \\ \Gamma \end{pmatrix} = \begin{pmatrix} (C + M - F)\tau_k + (F - C)\tau_g \\ (D + M - F)\tau_j + (F - D)\tau_h \end{pmatrix} \tag{31}$$

where g, h, j and k are the latitudes of the southern tip of the northern barrier, the northern tip of the southern barrier and the southern and northern tips of the Kerguelen Island, respectively, and where Λ and Γ are the Kerguelen and Antarctic streamfunctions.

The solution is shown in Fig. 9. This exhibits two eastward jets: one which passes north of the Kerguelen Island and one which passes to its south. The branches enter a western boundary current east of the island proceed as two distinct jets into Drake Passage.

The equivalent barotropic solution in Fig. 8 shares a number of these features. There are western boundary currents off South America and the Kerguelen plateau, and two branches in the longitude range between those features. Both branches enter the western boundary east of Kerguelen, and there are indications of two branches entering Drake Passage.

Increasing z_0 to 1100 m (not shown) further develops the Kerguelen barrier. The southern tip of the barrier now extends south nearly to Antarctica, with the result that the southern branch of the ACC is much weaker; most of the flow now passes north of the Kerguelen Plateau. The transport in this solution is still large, at 345 Sv.

Increasing z_0 to 1400 m increases these tendencies, closing the gap between the northern and southern portions of the Kerguelen Plateau and that between the southern tip and Antarctica (Fig. 10). Now nearly all the ACC passes north of the Kerguelen Plateau. In addition, the current exhibits more "wiggles", reflecting the greater influence of bottom topography. The transport is 230 Sv.

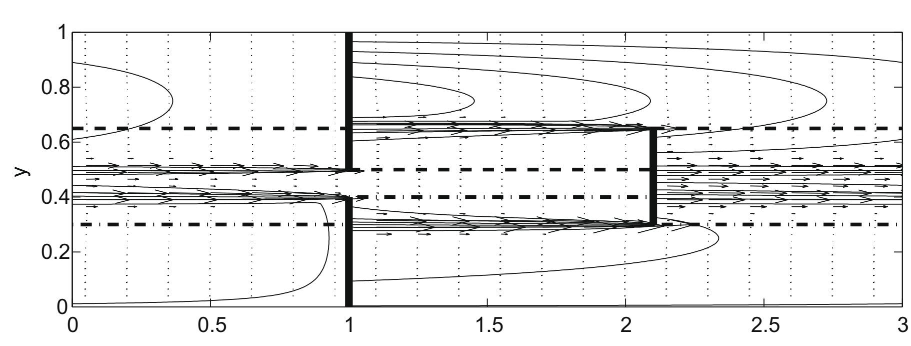

Fig. 9. The solution with the broken barrier model using a barrier configuration similar to that in Fig. 8. The friction coefficient is $\delta = 0.0002$ and the two island contours are indicated by the dashed and dash-dot lines.

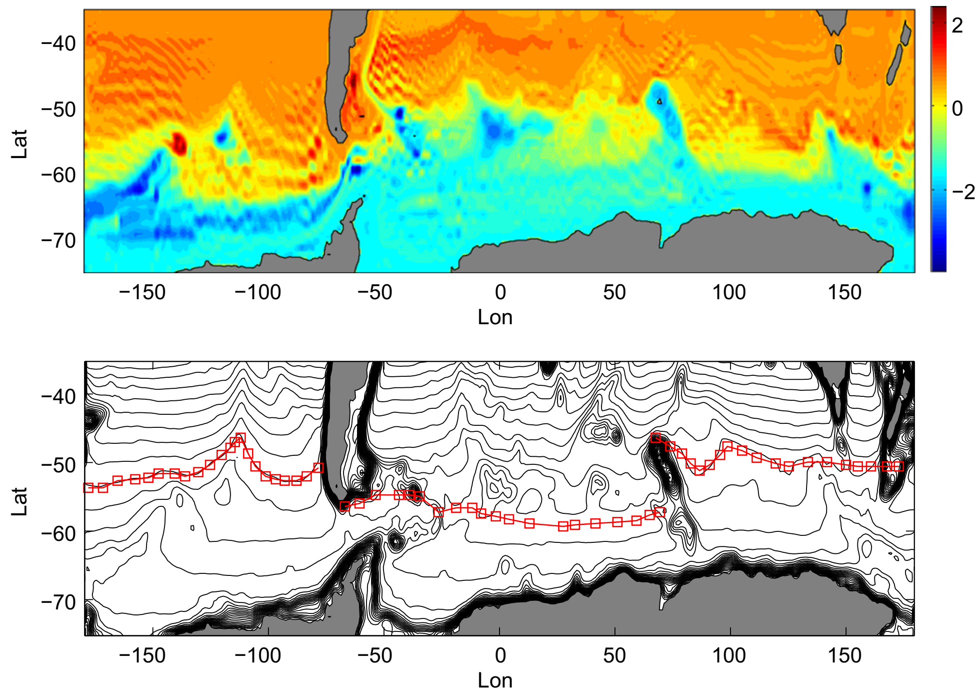

Fig. 10. Sea surface height from an equilibrated simulation with $z_0 = 1400$ m and $R = 10^{-5}$ m/s. The squares indicated the contour used in the island integral.

With the Kerguelen joined to Antarctica, this case is similar to Ishida's (1994) original configuration (Section 3). A corresponding solution is shown in Fig. 11. Here again there is only one unknown (the transport on Antarctica) and a single jet. The jet passes from South America to the northern tip of the plateau before moving south again. This is superimposed on gyres which close in western boundary currents to the east of the barriers.

As the Kerguelen Plateau is now the southern barrier, it is shifted east from where it would be if the latter represented the Scotian Island Arc. However, since the transport is only weakly dependent on the longitudinal separation between the barriers, this should have little effect. More important is the change in the meridional overlap, because the northern tip of the Kerguelen Plateau is nearly 10° north of the southern tip of South America. Following the discussion in Section 3, this greater separation favors a more inviscid jet. Note too that the Scotian Island Arc is largely passive in this solution; while it alters the gyre structure locally, it is unimportant for the transport of the ACC. The same is true for the Cambell plateau, which supports a western boundary current but does not affect the net transport.

If this solution is representative of the equivalent barotropic one in Fig. 10, we would expect the transport in the latter case to asymptote to a constant value with small drag coefficients. This is the case. Shown in Fig. 12 is the transport with $z_0 = 1400$ m over a range of R. With vanishing friction, the transport asymptotes to a value of around 230 Sv. If the model were in the Gill limit, the transport would vary inversely with R.

It should also be possible to estimate the transport in the inviscid limit using an island integral. For this, we require an island integral along f/F contours rather than latitude lines. To obtain this, we divide the momentum Eq. (4) by F and integrate along contours of constant f/F:

$$\oint \frac{\vec{\tau}}{\rho F} \cdot d\hat{l} = -\frac{f}{F} \oint \frac{\partial \psi}{\partial l} dl \tag{32}$$

Recall that for the inviscid limit, we neglect the frictional contribution.

We evaluate (32) by integrating numerically along the path indicated in Fig. 10. This consists of two f/F contours, aligned with the southern tip of South America (near 50S) and the northern tip

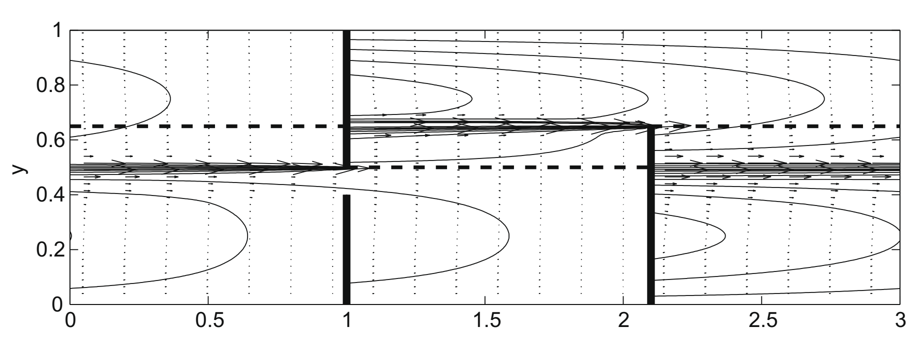

Fig. 11. The solution with the broken barrier model using a barrier configuration similar to that in Fig. 10. The friction coefficient is $\delta = 0.0002$ and the island contour is indicated by the dashed line.

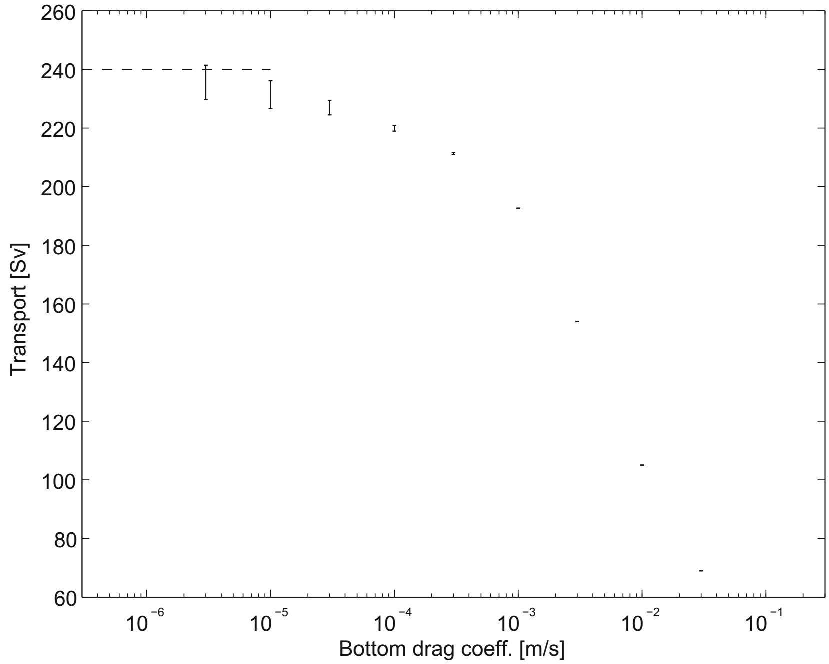

Fig. 12. Transport in Drake Passage vs. the bottom friction coefficient for the solution with $z_0 = 1400$ m. The transport has been averaged over the final third of the model run, and the error bars indicate the variation about the mean.

of the Kerguelen Plateau (near 60S). We use approximate f/F contours for this, neglecting the portions near the coasts and islands (as in the Scotian Arc). For the contour indicated in Fig. 10, we obtain an estimate of 240 Sv (using adjacent f/F contours produces estimates in the range from 220 to 260 Sv). Thus this estimate is consistent with the 230 Sv obtained numerically for Fig. 10.

Increasing z_0 further yields even more contorted f/F contours in the Drake latitudes. With $z_0 \approx 2000$ m (not shown), most of the f/F contours in Drake Passage turn back toward the South Pacific. The solution with $z_0 = 3000$ m (Fig. 13) is essentially steered by f/H contours. This solution corresponds to Kamenkovich's (1962) barotropic solution. We find that the transport through Drake Passage is about 50 Sv. A similar value was obtained by Krupitsky et al. (1996) in a solution using the shallow water vorticity equation.

Thus the EB model exhibits the dynamics of *all three* of the flat bottom analytical models. With z_0 less than about 600 m, the Drake Passage latitudes are open and the flow is like that in the Gill (1968) model. With z_0 between roughly 600 and 2000 m, the mod-

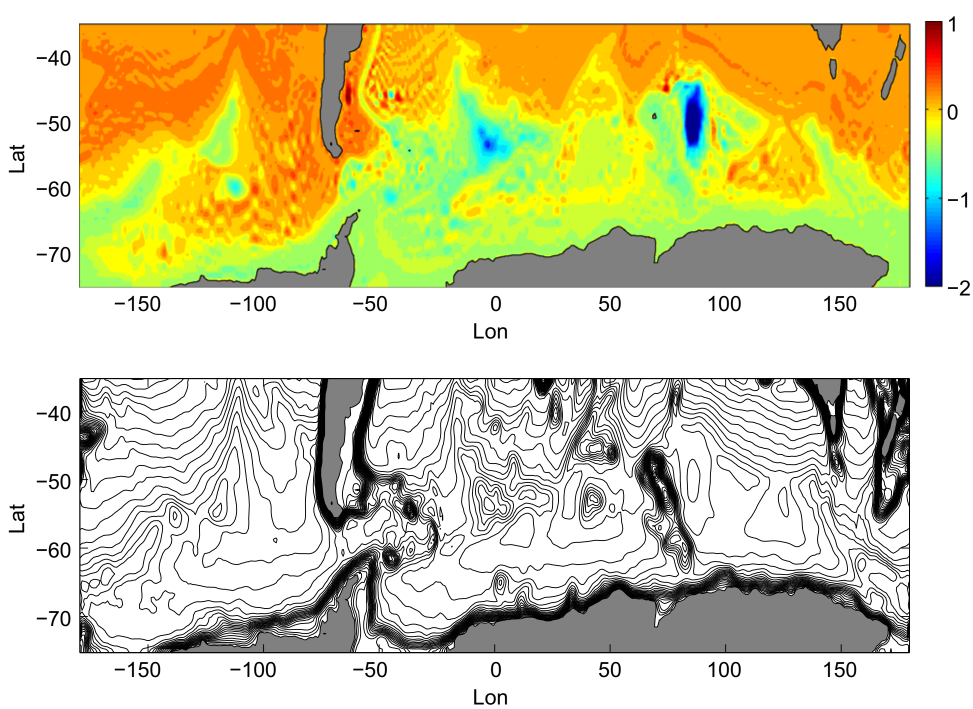

Fig. 13. Sea surface height from an equilibrated simulation with $z_0 = 3000$ m and $R = 10^{-5}$ m/s.

Please cite this article in press as: LaCasce, J.H., Isachsen, P.E. The linear models of the ACC. Prog. Oceanogr. (2010), doi:10.1016/j.pocean.2009.11.002

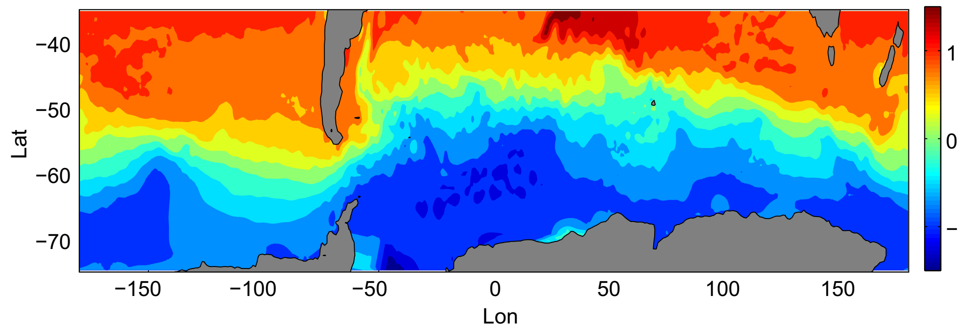

Fig. 14. Mean dynamic sea level height (in m) from the Rio and Hernandez (2004) climatology.

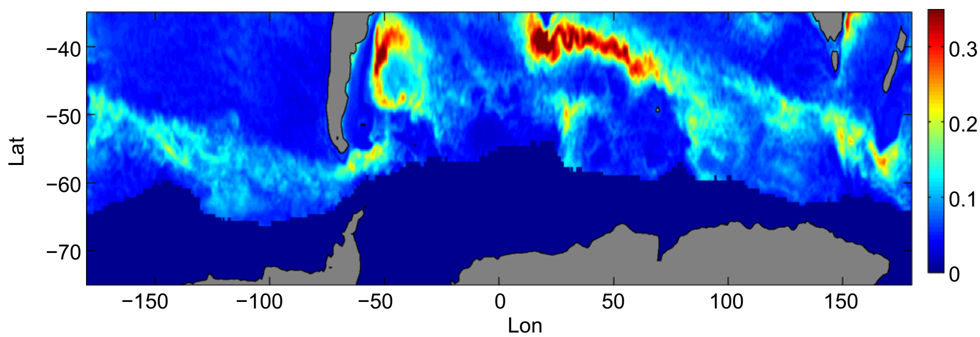

Fig. 15. RMS sea surface height variability (in m) from satellite altimetry. Derived from sea level anomalies produced by Salto/Duacs and distributed by Aviso. Ice-covered regions are in dark blue. (For interpretation of the references to colour in this figure legend, the reader is referred to the web version of this article.)

el resembles Ishida's (1994), with the geostrophic contours blocked by the Kerguelen Plateau. And with larger z_0, the contours are essentially f/H contours, as in Kamenkovich's (1962) solution.

Killworth (1992) suggested the e-folding scale for $P(z)$ was around 1200 m for the FRAM model and Killworth and Hughes (2002) found a somewhat larger value for the OCCAM simulation. Gille (2003) deduced a smaller value (700 m), by comparing trajectories of subsurface floats in the Southern Ocean with f/F contours. Nevertheless, all three estimates would put the ACC in the blocked contour regime.

6. Comparing the EB model to observations

The mean sea surface height in the Southern Ocean, from the Rio and Hernandez (2004) climatology, is shown in the upper panel of Fig. 14. Most of the features seen here are also found in the EB solution with intermediate z_0 (e.g. Fig. 10). The flow deviates 10° to the north along the eastern coast of South America and then proceeds eastward to 50E, the longitude of the Kerguelen Plateau. Thereafter it moves southeast, at least partially in a boundary current east of the Plateau.[5] It then rounds the Cambell Plateau south of New Zealand in another boundary current, before returning to the southern tip of South America.

However, there are also differences with the EB solution. The latter is "too wiggly", indicating too strong steering by topography. The western boundary current on the eastern side of the Kerguelen is sharper in the model than in the observations, and the gradients in the solution are generally too strong. Moreover, the transport (230 Sv) is roughly 50% larger than the 150 Sv observed in Drake Passage (Whitworth et al., 1982; Whitworth and Petersen, 1985; Cunningham et al., 2003).

If the e-folding scale really is around 1400 m, the actual ACC must be more viscid than in the weak friction limit. Increasing the bottom friction will reduce the transport, but we require $R \approx 5 \times 10^{-3}$ m/s to obtain a reasonable transport (Fig. 12); this is roughly an order of magnitude larger than expected (e.g. Gill, 1982; Isachsen et al., 2003). Moreover, increasing the bottom drag will not alter the wiggliness of the solution because linear drag acts equally on all scales.

6.1. Lateral diffusion

A way to address both issues is to include lateral eddy stirring. Indeed, it is well-known that the ACC is unstable, with eddies generated along nearly its entire path. This can be seen in Fig. 15, which shows the rms variability in the sea surface height. The largest variability occurs off the coast of South America and in the Agulhas Retroflection, but there is enhanced variability in many other regions as well. While the model does not permit instability, we can mimic the eddy stirring by including a lateral diffusion term (as in Munk's (1950) model of the North Atlantic). Specifically, we add a diffusion term to the model momentum equations, which results in a lateral diffusion of relative vorticity.[6]

An example is shown in Fig. 16. This has $z_0 = 1400$ m, a bottom friction coefficient of $R = 5 \times 10^{-4}$ m/s and a lateral diffusion coefficient of 3×10^3 m^2/s. The latter is in line with estimates derived from surface drifters in the Southern Ocean (Sallee et al., 2008). The resulting solution compares quite well with the observed field in Fig. 14, even though the solution still exhibits stronger gradients than observed and is more strongly influenced by topography. The transport in this solution is 170 Sv, somewhat larger than, but comparable to, observations. Of course, the transport would

[5] The western boundary current east of the Kerguelen Plateau is discussed by Speer and Forbes (1994) and Donohue et al. (1999).

[6] More properly, one could diffuse potential vorticity (e.g. Treguier et al., 1997). Both approaches however will act to smooth the small scales.

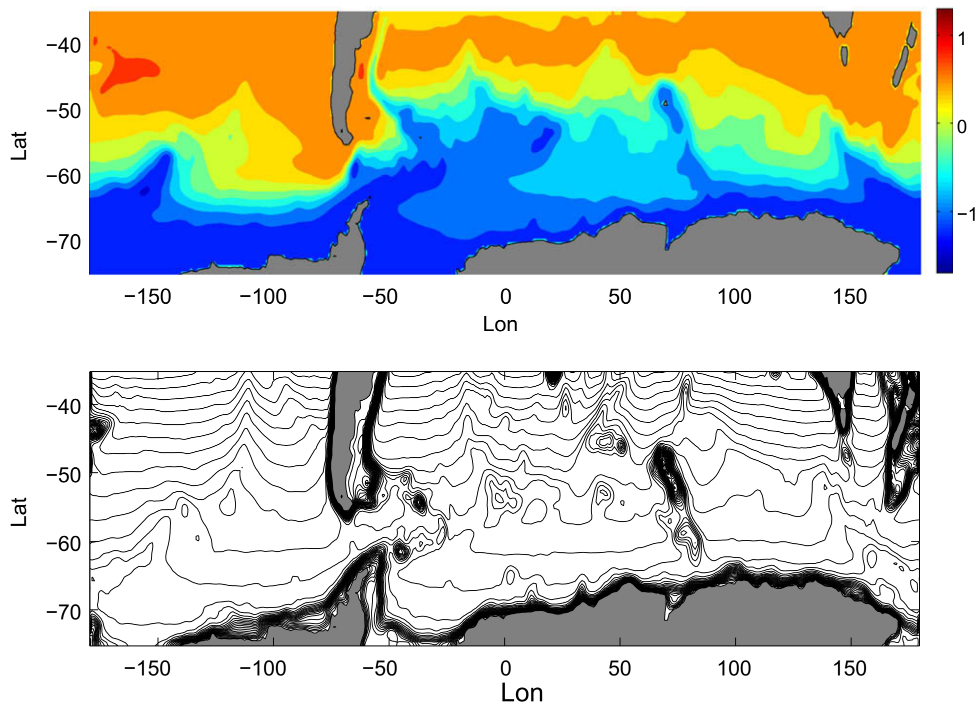

Fig. 16. Surface height contours from a solution with additional lateral dissipation, with $z_0 = 1400$ m, $R = 5 \times 10^{-4}$ m/s and $\nu = 3 \times 10^3$ m^2/s.

be reduced further with a larger viscosity. It is also reduced by about 10% using the SOC winds. But the similarity with Fig. 14 suggests the model is not far from reality. We conclude that eddy mixing is probably important in determining the horizontal structure of the ACC.

6.2. Wind stress curl

As noted in the beginning, Stommel (1957) suggested the transport of the ACC could be estimated by a circumpolar integral of the wind stress curl and a number of subsequent studies supported this (Baker, 1982; Godfrey, 1989; Chelton et al., 1990; Warren et al., 1996). If the present results are correct, this agreement must be coincidental, because the transport should be determined instead by the wind stress.

We rechecked the Sverdrup estimate, using three different wind products: the Trenberth et al. (1989) climatology, the Southampton SOC GASC97 product (Josey et al., 1999) and Hellerman and Rosenstein's (1983) climatology. We integrated the curl at 55S with each set. The resulting transport was negative (southward) for both the Hellerman and Rosenstein and Trenberth products and roughly 100 Sv in both cases. The transport from the SOC product on the other hand was not different from zero; this is because the zero curl line in the SOC product coincides with the South American tip. Thus the agreement between the integrated curl and the ACC transport appears to depend on the choice of winds.

7. Comparing the EB model to GCMs

The EB model also shows distinct similarities to solutions obtained with general circulation models. This is well-illustrated in the article by Ivchenko et al. (1999), who compared an EB solution with output from the FRAM simulation. In particular, the EB model produced a similar mean streamfunction (albeit with somewhat sharper lateral gradients, as in the preceding section) and transport (of 180 Sv).

7.1. Form drag

In addition, Ivchenko et al. demonstrated that the EB model exhibits a form drag balance very much like that in FRAM. This balance derives from the the steady depth- and zonally-integrated x-momentum equation. Written in Cartesian coordinates, this is:

$$\oint \int_{-H}^{0} \frac{\partial}{\partial y}(vu)\,dzdx = \oint \int_{-H}^{0} \frac{1}{\rho}\frac{\partial p}{\partial x}\,dzdx + \oint \frac{\tau_x(0)}{\rho}\,dx - \oint Ru\,dx + \mathscr{R} \tag{33}$$

where $\mathscr{R}$ is a residual which includes all neglected terms, such as lateral dissipation and the vertical advection of momentum. Note that the Coriolis and zonal advection of momentum terms vanish in the circumpolar integral. The pressure term can be rewritten using Leibniz's rule:

$$\oint \int_{-H}^{0} \frac{1}{\rho}\frac{\partial p}{\partial x}\,dzdx = \oint \frac{\partial}{\partial x}\int_{-H}^{0} \frac{p}{\rho}\,dzdx + \oint \frac{1}{\rho}p(-H)\frac{\partial H}{\partial x}\,dx \tag{34}$$

and the first term on the RHS vanishes. So the zonal integral is:

$$\oint \int_{-H}^{0} \frac{\partial}{\partial y}(vu)\,dzdx = \oint \frac{1}{\rho}p(-H)\frac{\partial H}{\partial x}\,dx + \oint \frac{\tau_x(0)}{\rho}\,dx - \oint Ru\,dx + \mathscr{R} \tag{35}$$

As noted previously, diverse numerical studies of the Southern Ocean indicate there is an approximate balance between the wind stress and bottom pressure terms, the first two terms on the RHS of (35). This suggests the zonal stress exerted by the wind at the surface is balanced by pressure differences across topography. However, there is another way of viewing this. The bottom pressure term can be rewritten following integration by parts:

$$\oint \frac{1}{\rho}p(-H)\frac{\partial H}{\partial x}\,dx = -\oint \frac{H}{\rho}\frac{\partial p(-H)}{\partial x}\,dx = -\oint fHv_g(-H)\,dx \tag{36}$$

where $v_g(-H)$ is the geostrophic meridional velocity at the bottom. Note the last integral does not vanish because the integration path proceeds between topographic features (it is below the "sill depth").

Please cite this article in press as: LaCasce, J.H., Isachsen, P.E. The linear models of the ACC. Prog. Oceanogr. (2010), doi:10.1016/j.pocean.2009.11.002

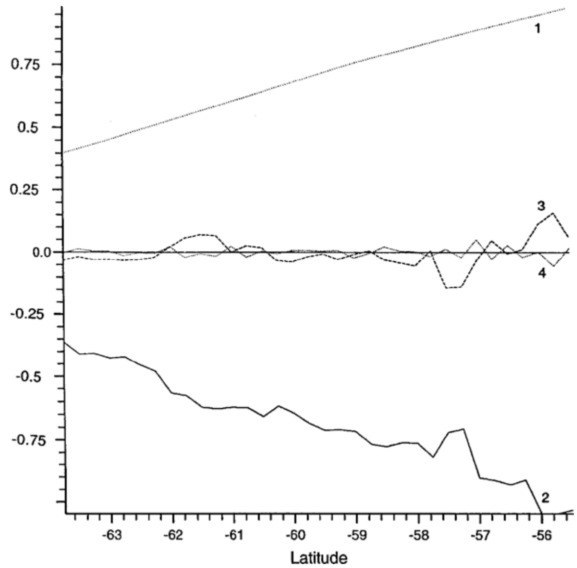

Fig. 17. The zonally-averaged, time–mean zonal momentum balance in the FRAM simulation. Lines (1) and (2) correspond to the wind stress and bottom form drag, and lines (3) are (4) are the poleward momentum flux divergence and the residual terms. The units are 10^{-4} m^2/s^2. From Stevens and Ivchenko (1997), with permission.

So the form drag balance is equivalently a balance between the surface Ekman transport and the geostrophic meridional transport near the bottom (Warren et al., 1996).

Integral (35), evaluated with the FRAM data, is shown in Fig. 17. The wind stress and bottom pressure terms are by far the largest, with the advective and residual terms being much smaller (Stevens and Ivchenko, 1997). Ivchenko et al. (1999) demonstrated that the EB model exhibits the same balance. The wind stress and bottom pressure terms dominate, with the bottom friction playing a secondary role.

We illustrate the latter with the present EB model in Fig. 18. Note that our version of the EB model differs in several ways from that of Ivchenko et al.; we use a different vertical structure function, $P(z)$, with weaker bottom velocities, and use a smaller bottom friction coefficient. The terms shown in Fig. 18 derive from the solution in Fig. 16. As in Fig. 17, the wind stress and bottom pressure terms nearly balance one another. The three other terms (lateral and bottom friction, and the residual) are considerably smaller. Bottom friction is actually less important here even than in Ivchenko et al. (1999), probably because of the differences sited above.

Thus the EB model captures the form drag balance seen in many numerical models. However, form drag *does not reveal the transport of the ACC.* While form drag derives from an integral of a momentum equation, like the island integral used in Section 5, it is along a latitude line. It is thus, effectively, along the wrong contour. In order to estimate the transport, the integral must be along f/F contours.

The EB model predicts—in both the closed and blocked contour regimes—that the strength of the ACC is determined by the wind stress, not the curl. Gnanadesikan and Hallberg (2000) examined this question explicitly, with coarse resolution simulations of the GFDL MOM model. They ran simulations varying the wind stress while holding the curl constant, and vice versa. The results (Fig. 19) suggested the ACC transport was linearly dependent on the wind stress. However it was independent of the curl.

In addition, Gnanadesikan and Hallberg (2000) found that the Sverdrup balance was approximately satisfied at points in the Southern Ocean interior. This, and the transport dependence on the wind stress, are in agreement with the Ishida (1994) model and the EB model in the blocked geostrophic contour regime.

Gnanadesikan and Hallberg (2000) also showed that thermohaline forcing was important for the ACC transport. In their model, thermohaline forcing, with its associated upwelling of dense water, alters the cross stream density gradient and hence the thermal wind balance in the ACC. In the context of the EB model, we would say that thermohaline forcing alters z_0, the vertical scale of the current, as the vertical shear is linked to the lateral density gradient by

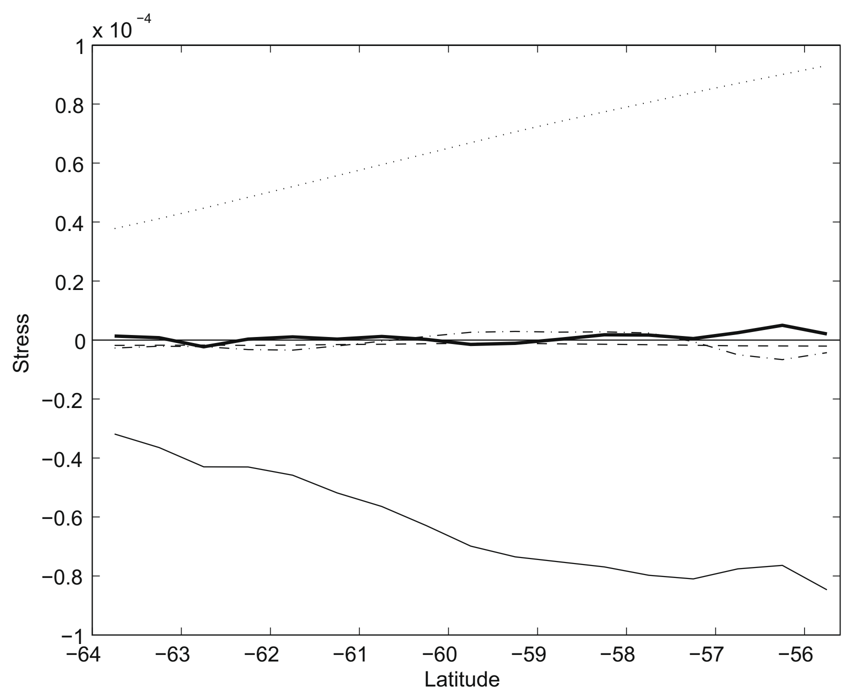

Fig. 18. The form drag balance calculated for the EB solution shown in Fig. 16 in the Drake Passage latitudes. The terms are wind stress (dotted line), bottom pressure (solid), lateral friction (dash-dot), bottom friction (dashed) and residual (thick solid).

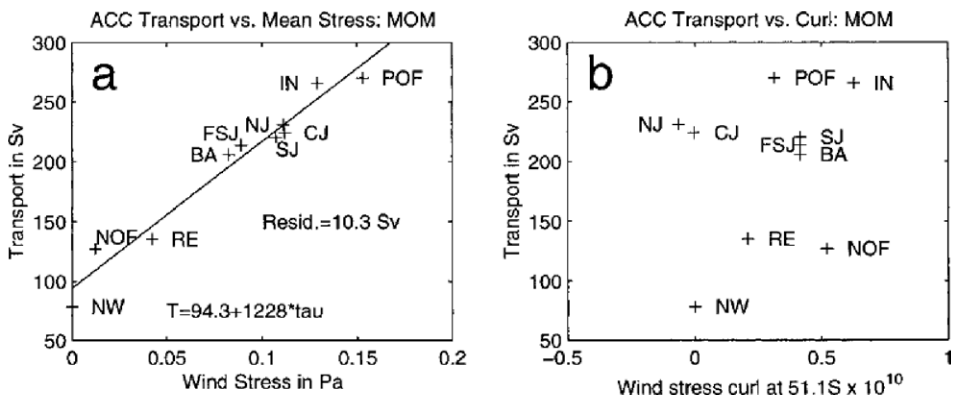

Fig. 19. Regression of the ACC transport vs. wind stress (left panel) and curl (right panel) in the Drake Passage latitudes in the GCM calculations of Gnanadesikan and Hallberg (2000). Reprinted with permission.

thermal wind. However z_0 is set in the EB solution; it is not an unknown.

8. Summary and discussion

We have examined the linear, wind-driven models of the ACC. We began with two barotropic, flat bottom channel models. Gill's (1968) model has blocked latitude lines in the north and unblocked lines in the south, and yields a circumpolar current whose transport varies inversely with the bottom drag coefficient. This transport is also too large for reasonable values of that coefficient. Ishida's (1994) model, in which the lines are blocked at all latitudes by two disconnected barriers, also yields a circumpolar jet. But in this case the transport asymptotes to a constant value with vanishing bottom drag.

We then examined Krupitsky et al.'s (1996) equivalent barotropic model with topography. The model assumes the velocities have a self-similar vertical structure which is assumed to be exponential. We then examined how the solutions depend on the vertical e-folding scale, z_0. The central point is that the choice of z_0 affects the geostrophic contours, because it determines to what extent the current feels the topography. For $z_0 \lesssim 600$ m, the solution resembles that in the Gill model because the geostrophic contours in the Drake Passage latitudes are nearly zonal and hence closed. With $600 \lesssim z_0 \lesssim 2000$ m, the flow is deep enough so that the geostrophic contours are blocked by the Kerguelen Plateau. Then the solutions are like those in the Ishida model, with a circumpolar transport which asymptotes to a constant value with vanishing bottom drag. With $z_0 \gtrsim 2000$ m, the geostrophic contours are essentially f/H contours and are dominated by topography. In this limit, the model is like the barotropic model considered by Kamenkovich (1962).

Results from the FRAM model (Killworth, 1992) and the OCCAM model (Killworth and Hughes, 2002) suggest the actual e-folding scale is around 1200 m, which would put the ACC in the blocked barrier regime, as in Ishida's (1994) model. This would imply that the transport is insensitive to the choice of bottom friction coefficient, provided it is small enough. That asymptotic limit can in principle be estimated analytically using a contour integral. With an e-folding scale of 1400 m, we obtained an estimate of 240 Sv, similar to the value obtained by solving the equivalent barotropic system numerically.

The fact that this value is roughly 50% larger than observed suggests that additional friction is required. This is most likely due to lateral dissipation, induced by eddies along the path of the ACC. Including lateral friction with a reasonable viscosity reduces the transport to a value within range of the observations. The resulting solution bears a strong resemblance to the mean sea surface height from satellite observations (Rio and Hernandez, 2004).

The present results thus support Stommel's (1957) assertion that the geostrophic contours in the Southern Ocean are blocked (although the Kerguelen Plateau is the primary barrier, rather than the Scotian Island Arc). These results also support the idea that the interior is near Sverdrup balance. But the transport of the ACC is not determined by the integrated wind stress curl, but by the integrated wind stress. Gnanadesikan and Hallberg (2000) reached the same conclusion in an analysis of a suite of GCM solutions.

The present results also counter the notion that the ACC is primarily a zonal current. Because the geostrophic contours are blocked, western boundary currents and the associated meridional deviations of the jet are critically important. A Sverdrup interior is impossible in a pure channel configuration. This throws doubt on the relevance of channel and zonally-averaged models of the current. Munk and Palmen (1951) suggested that the primary dynamical balance in the ACC is between the eastward stress exerted by the wind at the ocean surface and pressure differences across bottom topography, the form drag balance. Subsequent numerical studies have supported this notion. However, the EB model also exhibits a form drag balance which is fully comparable to that seen in full GCMs (Ivchenko et al., 1999). We note that the reason for this is that the form drag integral is like the island integral which determines the strength of the ACC in the Ishida and EB models. However, being a zonal integral, the form drag balance effectively employs the wrong contour of integration. It is for this reason that it cannot determine the ACC transport.

A central question with regards to the EB model is what determines the vertical scale, z_0. From the results of Gnanadesikan and Hallberg (2000), it may be that thermohaline forcing is important as it could alter the density gradients across the ACC. Consistent with this, they found that thermohaline forcing affected the total transport in their simulations. But z_0 could also be affected by eddies, which act to redistribute density across the stream while reducing the vertical shear.

In effect, the EB model tells us how the ACC responds to topography, once the stratification has been established, but it does not tell us how the latter comes about. There is a parallel in the atmospheric literature. Models which are linearized about the time–mean zonal circulation are effective at describing the tropospheric response to orographic and thermal forcing at the lower boundary (e.g. Held et al., 2002). But these models cannot say what determines the zonal mean flow. The latter, which involves the forcing of the mean by the eddies generated by the instability of the mean, is a fully nonlinear process.

However, it is worth remembering that the barotropic models of the subtropical gyres likewise fail to determine the vertical stratification. That is set by thermohaline forcing, vertical pumping by the winds and possibly also by lateral eddy transport. So the situation in the Southern Ocean may well be like that in the subtropical gyres.

While the EB model is a compelling one for the ACC, there remain several questions about its application. These could be addressed by further comparisons between the model and GCMs, like that undertaken by Ivchenko et al. (1999). For example, we employed a crude representation of baroclinic instability in the model, a downgradient diffusion of relative vorticity with a constant diffusivity. The actual situation is most certainly more complicated and could be elucidated with a high resolution model.

Such a model comparison could also help explain why the smaller topographic scales do not seem to matter for the large scale structure. It is possible, for example, that the scales below that of the baroclinic eddies will necessarily be "washed out". Because the geostrophic contours are sensitive to the details of the bottom topography, topographic smoothing can alter the transport. For example, by smoothing at the 500 km scale Krupitsky et al. (1996) obtained *closed* f/F contours. They therefore required larger values of bottom friction to obtain a reasonable transport, as with Gill's (1968) model. Using a smaller smoothing scale, we obtain contours which are mostly blocked. Thus topographic smoothing may also account for the overly large ACC transports seen in coarse resolution numerical simulations, such as with FRAM and the simulations studied by Gnanadesikan and Hallberg (2000).

There is also the question of what constitutes a blocked contour. In the cases with $z_0 \gtrsim 800$ m, the Kerguelen Plateau effectively blocks the contours in the Drake Passage latitudes. In fact, these contours wrap around the Plateau (as expected, since $F \rightarrow H$ in shallow water). Why then are these contours blocked at all? In particular, what differentiates a barrier and a bump, if the latter only causes the current to deviate and does not support a western boundary current? It may be that the answer concerns the relative widths of topographic slope and those of the Stommel/Munk layers (see for example the recent work by Pedlosky et al. (2009)). If so, this will also affect the choice of topographic smoothing scale and of friction.

In any case, the equivalent barotropic model yields promising solutions. We agree with Ivchenko et al. (1999) that the model deserves further attention and could even be used for interpreting observations.

Acknowledgments

We have enjoyed many conversations with Joe Pedlosky, and George Veronis urged us to include lateral diffusion in the EB solution. We also received helpful comments from two anonymous reviewers. The work was supported by the Bipolar Atlantic Thermohaline Circulation (BIAC) project, funded by the Norwegian Research Council.

Appendix A

The solution to Ishida's (1994) model can be obtained in four steps. The first is to integrate the Sverdrup relation (15) west from the eastern boundary at each latitude. The second is to add Stommel boundary layer corrections at each of the western boundaries. Then zonal boundary layer corrections are added to smooth discontinuities along the dashed lines in Fig. 1. Finally, the island rule integral (37) is calculated to determine the streamfunction on Antarctica, Γ.

The streamfunction is calculated in six regions, as indicated in Fig. 20. The western boundary layers occur in regions II, III, IV and VI, and the zonal boundary layers are along the dotted lines in the figure. The latter corrections have the form of a complimentary error function.

The solutions by region are as follows. Using $W = -\frac{\partial}{\partial y}\tau^x$ to indicate the wind stress curl, we have:

$$\psi_{\mathrm{I}} = (x - C)W - \frac{1}{2}[(D - C)W - \Gamma]erfc\left(\frac{y - g}{2\sqrt{\delta(C - x)}}\right)$$

$$\psi_{\mathrm{II}} = (x - M - C)W + MWexp\left(-\frac{x - C}{\delta}\right) - \frac{1}{2}[(D - M - C)W - \Gamma]erfc\left(\frac{y - h}{2\sqrt{\delta(D - x)}}\right)$$

$$\psi_{\mathrm{III}} = (x - D)W + \Gamma + [(D - C)W - \Gamma]exp\left(-\frac{x - C}{\delta}\right) + \frac{1}{2}[(D - C)W - \Gamma]erfc\left(\frac{y - h}{2\sqrt{\delta(D - x)}}\right)$$

$$\psi_{\mathrm{IV}} = (x - M - C)W + (M + C - D)Wexp\left(-\frac{x - D}{\delta}\right) - \frac{1}{2}[(D - C)W - \Gamma]erfc\left(\frac{y - g}{2\sqrt{\delta(M + C - x)}}\right)$$

$$\psi_{\mathrm{V}} = (x - D)W + \Gamma + \frac{1}{2}[(D - C)W - \Gamma]erfc\left(\frac{y - g}{2\sqrt{\delta(C - x)}}\right)$$

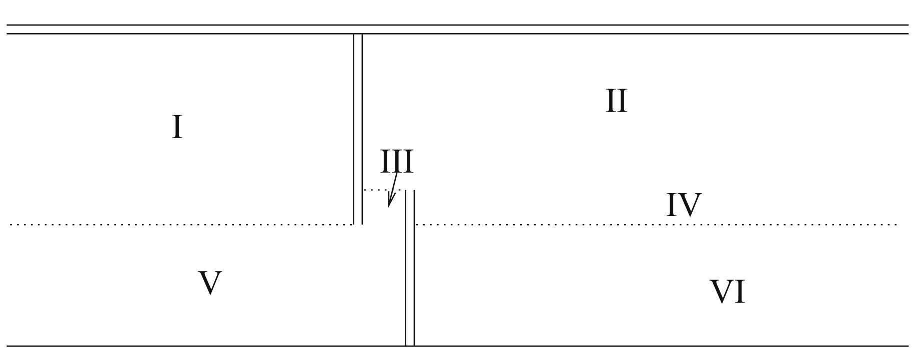

Fig. 20. The different domains in which the Sverdrup integral is evaluated. Discontinuities occur along the dotted lines, resulting in zonal boundary layers.

Please cite this article in press as: LaCasce, J.H., Isachsen, P.E. The linear models of the ACC. Prog. Oceanogr. (2010), doi:10.1016/j.pocean.2009.11.002

$$\psi_{\rm VI} = (x - M - D)W + \Gamma + [MW - \Gamma]exp\left(-\frac{x-D}{\delta}\right) + \frac{1}{2}[(D-C)W - \Gamma]erfc\left(\frac{y-g}{2\sqrt{\delta(M+C-x)}}\right)$$

The transport, Γ, is found from (22). Only the two zonal segments contribute, and the integrals take the form:

$$-\hat{f}(y)\int_A^B \frac{\partial}{\partial x}\psi dx = \hat{f}(y)[\psi(A) - \psi(B)] = \int \tau^x dx + \delta\int_A^B \frac{\partial}{\partial y}\psi dx \tag{37}$$

where A and B and the end points of the segment. As noted in the text, we retain the frictional term because the zonal boundary layers can overlap the island contours.[7]

The term on the LHS of (37), with contributions from all three zonal segments, can be shown to be:

$$\Gamma[\hat{f}(b) - \hat{f}(a)] \tag{38}$$

while the wind stress term reduces to:

$$\tau(b)M + [\tau(a) - \tau(b)](D - C) \tag{39}$$

(the various constants are given in Fig. 1). The frictional term on the other hand requires the full solution for ψ. The final result is:

$$\Gamma = \frac{N}{D} \tag{40}$$

where the numerator is:

$$N = \tau(b)E + \tau(a)(D-C) - \frac{\partial}{\partial y}W(b)\left[\frac{\delta E^2}{2} + (D-C)\frac{(h-g)^2}{8\gamma^2}erfc(\gamma)\right] - \frac{\partial}{\partial y}W(a)\left[\frac{\delta(C-D)^2}{2} + E\frac{(h-g)^2}{8\alpha^2}erfc(\alpha)\right] + \frac{h-g}{2\sqrt{\pi}}(D - C)\left[\frac{\partial}{\partial y}W(b)\frac{h-g}{2} + W(b)\right]\left(\frac{1}{\gamma}exp(-\gamma^2) - \sqrt{\pi}[1 - erf(\gamma)]\right) + \frac{h-g}{2\sqrt{\pi}}E\left[\frac{\partial}{\partial y}W(a)\frac{h-g}{2} + W(a)\right] \times \left(\frac{1}{\alpha}exp(-\alpha^2) - \sqrt{\pi}[1 - erf(\alpha)]\right)$$

and the denominator is:

$$D = \hat{f}(b) - \hat{f}(a) - \frac{h-g}{2\sqrt{\pi}}\left[\frac{1}{\alpha}exp(-\alpha^2) - \frac{1}{\gamma}exp(-\gamma^2) + \sqrt{\pi}(erf(\alpha) - erf(\gamma))\right]$$

We have defined the constants:

$$\gamma = \frac{h-g}{2\sqrt{\delta(D-C)}}, \quad \alpha = \frac{h-g}{2\sqrt{\delta E}}, \quad E = M + C - D$$

Note the transport has a nonlinear dependence on the bottom friction coefficient; this stems from the meridional spreading of the zonal boundary layers.

References

Baker, D.J., 1982. A note on Sverdrup balance in the Southern Ocean. J. Mar. Res. 40 (Suppl.), 41–46.
Bryan, K., 1963. A numerical investigation of a non-linear model of a wind-driven ocean. J. Atmos. Sci. 69, 27–40.
Carlson, T.N., 1991. Mid-latitude Weather Systems. Harper-Collins. 483 pp.

[7] A similar situation is discussed by Pedlosky et al. (1997) with regards to an island integral around a zonally-elongated island, due to frictional layers on the north and south sides of the island.

Charney, J.G., 1949. On a physical basis for numerical prediction of large-scale motions in the atmosphere. J. Atmos. Sci. 6, 372–385.
Chelton, D.B., Mestas-Nunes, A.M., Freilich, M.H., 1990. Global wind stress and Sverdrup circulation from the Seasat scatterometer. J. Phys. Oceanogr. 20, 1175–1205.
Cunningham, S.A., Alderson, S.G., King, B.A., Brandon, M.A., 2003. Transport and variability of the Antarctic Circumpolar Current in Drake Passage. J. Geophys. Res. 108, 8084. doi:10.1029/2001JC001147.
Donohue, K.A., Hufford, G.E., McCartney, M.S., 1999. Sources and transport of the Deep Western Boundary Current east of the Kerguelen Plateau. Geophys. Res. Lett. 26, 851–854.
Fjørtoft, R., 1952. On a numerical method of integrating the barotropic vorticity equation. Tellus 4, 179–194.
FRAM Group, 1991. An eddy-resolving model of the Southern Ocean. EOS Trans. Am. Geophys. Union 72, 169–175.
Gent, P.R., Large, W.G., Bryan, F.O., 2001. What sets the mean transport through Drake Passage. J. Geophys. Res. 106, 2693–2712.
Gill, A.E., 1968. A linear model of the Antarctic Circumpolar Current. J. Fluid Mech. 32, 465–488.
Gill, A.E., 1982. Atmosphere-Ocean Dynamics. Academic Press. 662 pp.
Gille, S.T., 1997. The Southern Ocean momentum balance: evidence for topographic effects from numerical model output and altimeter data. J. Phys. Oceanogr. 27, 2219–2232.
Gille, S.T., 2003. Float observations of the Southern Ocean: part I, estimating mean fields, bottom velocities and topographic steering. J. Phys. Oceanogr. 33, 1167–1181.
Gnanadesikan, A., Hallberg, R., 2000. On the relationship of the Circumpolar Current to Southern Hemisphere winds in coarse-resolution ocean models. J. Phys. Oceanogr. 30, 203–2034.
Godfrey, J.S., 1989. A Sverdrup model of the depth-integrated flow for the world ocean allowing for island circulations. Geophys. Astrophys. Fluid Dyn. 45, 89–112.
Greenspan, H.P., 1968. The Theory of Rotating Fluids. Camb. Univ. Press. 327 pp.
Hautala, S., Roemmich, D.H., Schmitz, W.J., 1994. Is the North Pacific in Sverdrup balance along 24 N? J. Geosphys. Res. 99, 16041–16052.
Held, I.M., Ting, M., Wang, H., 2002. Northern winter stationary waves: theory and modelling. J. Clim. 15, 2125–2144.
Hellerman, S., Rosenstein, M., 1983. Normal monthly wind stress over the world ocean with error estimates. J. Phys. Oceanogr. 13, 1093–1104.
Hughes, C.W., 2002. Sverdrup-like theories of the Antarctic Circumpolar Current. J. Mar. Res. 60, 1–17.
Isachsen, P.E., LaCasce, J.H., Mauritzen, C., Hakkinen, S., 2003. Wind-forced barotropic flow in sub-polar regions. J. Phys. Oceanogr. 33, 2534–2550.
Ishida, A., 1994. Effects of partial meridional barriers on the Antarctic Circumpolar Current – wind driven barotropic model. Dyn. Atmos. Oceans 20, 315–341.
Ivchenko, V.O., Krupitsky, A.E., Kamenkovich, V.M., Wells, N.C., 1999. Modeling the Antarctic Circumpolar Current: a comparison of FRAM and equivalent barotropic model results. J. Mar. Res. 57, 29–45.
Jayne, S.R., Hogg, N.G., 1999. On recirculation forced by an unstable jet. J. Phys. Oceanogr. 29, 2711–2718.
Johnson, J.A., Hill, R.B., 1975. Three-dimensional model of the Southern Ocean with bottom topography. Deep-Sea Res. 22, 745–751.
Josey, S., Kent, E., Taylor, P., 1999. New insights into the ocean heat budget closure problem from analysis of the SOC air-sea flux climatology. J. Clim. 12 (9), 2856–2880.
Kamenkovich, V.M., 1962. On the theory of the Antarctic Circumpolar Current. Trudy Instituta Okeanologii 56, 245–306.
Killworth, P.D., 1992. An equivalent-barotropic mode in the fine resolution Antarctic Model. J. Phys. Oceanogr. 22, 1379–1387.
Killworth, P.D., Hughes, C.W., 2002. The Antarctic Circumpolar Current as a free equivalent-barotropic jet. J. Mar. Res. 60, 19–45.
Krupitsky, A., Kamenkovich, V.M., Naik, N., Cane, M.A., 1996. A linear equivalent barotropic model of the Antarctic Circumpolar Current with realistic coastlines and bottom topography. J. Phys. Oceanogr. 26, 1803–1824.
Leetmaa, A., Niiler, P.P., Stommel, H.M., 1977. Does the Sverdrup relation account for the Mid-Atlantic circulation? J. Mar. Res. 35, 1–10.
Marshall, D.P., 1995. Topographic steering of the Antarctic Circumpolar Current. J. Phys. Oceanogr. 25, 1636–1650.
Munk, W.H., Palmen, E., 1951. Note on the dynamics of the Antarctic Circumpolar Current. Tellus 3, 53–55.
Olbers, D., Borowski, D., Volker, C., Wolff, J.-O., balance, The dynamical, 2004. transport and circulation of the Antarctic Circumpolar Current. Antarct. Sci. 16, 439–470.
Pedlosky, J., 1987. Geophysical Fluid Dynamics. Springer. 728 pp.
Pedlosky, J., Pratt, L.J., Spall, M.A., Helfrich, K.R., 1997. Circulation around islands and ridges. J. Mar. Res. 55, 1199–1251.
Pedlosky, J., Iacono, R., Napolitano, E., Helfrich, K., 2009. The skirted island: the effect of topography on the flow around planetary scale islands. J. Phys. Res.
Rintoul, S.R., Hughes, C.W., Olbers, D., 2002. The Antarctic Circumpolar Current system. In: Siedler, G., Church, J., Gould, J. (Eds.), Ocean Circulation and Climate, International Geophysical Series, vol. 77. Academic press.
Rio, M.-H., Hernandez, F., 2004. A mean dynamic topography computed over the world ocean from altimetry, in situ measurements and a geoid model. J. Geophys. Res. 109. doi:10.1029/2003JC002226.
Sallee, J.B., Speer, K., Morrow, R., Lumpkin, R., 2008. An estimate of Lagrangian eddy statistics and diffusion in the mixed layer of the Southern Ocean. J. Mar. Res. 66, 441–463.

Saunders, P.M., Coward, A.C., de Cuevas, B.A., 1999. Circulation of the Pacific Ocean seen in a global ocean model (OCCAM). J. Geophys. Res. 104, 18281–18299.

Shchepetkin, A.F., McWiliams, J.C., 2005. The regional oceanic modeling system (ROMS): a split-explicit, free-surface, topography-following-coordinate oceanic model. Ocean Model 9, 347–404.

Speer, K., Forbes, A., 1994. A deep western boundary current in the South Indian basin. Deep-Sea Res. 41, 1289–1303.

Stevens, D.P., Ivchenko, V.O., 1997. The zonal momentum balance in an eddy-resolving general-circulation model of the Southern Ocean. Quart. J. Roy. Met. Soc. 123, 929–951.

Stommel, H., 1948. The westward intensification of wind-driven ocean currents. Trans. Am. Geophys. Union 29, 202–206.

Stommel, H., 1957. A survey of ocean current theory. Deep-Sea Res. 4, 149–184.

Sun, C., Watts, D.R., 2001. A circumpolar gravest empirical mode for the Southern Ocean hydrography. J. Geophys. Res. 106, 2833–2855.

Treguier, A.M., McWilliams, J.C., 1990. Topographic influences on wind-driven, stratified flow in a β-plane channel: an idealized model for the Antarctic Circumpolar Current. J. Phys. Oceanogr. 20, 321–343.

Treguier, A.M., Held, I.M., Larichev, V.D., 1997. Parameterization of quasigeostrophic eddies in primitive equation ocean models. J. Phys. Oceanogr. 27, 567–580.

Trenberth, K., Olson, J., Large, W., 1989. A Global Ocean Wind Stress Climatology Based on ECMWF Analyses. Tech. Rep. NCAR/TN-338+STR, National Center for Atmospheric Research, Boulder, Colorado.

Vallis, G., 2006. Atmospheric and Oceanic Fluid Dynamics: Fundamentals and Large-scale Circulation. Camb. Univ. Press. 745 pp.

Veronis, G., 1966. Wind-driven ocean circulation—part 2. Numerical solutions of the nonlinear problem. Deep-Sea Res. 13, 31–55.

Warren, B.A., LaCasce, J.H., Robbins, P.E., 1996. On the obscurantist physics of "form drag" in theorizing about the circumpolar current. J. Phys. Oceanogr. 26, 2297–2301.

Webb, D.J., 1993. A simple model of the effect of the Kerguelan Plateau on the strength of the Antarctic Circumpolar Current. Geophys. Astrophys. Fluid Dyn. 70, 57–84.

Welander, P., 1968. Wind-driven circulation in one- and two-layer oceans of variable depth. Tellus 20, 1–15.

Whitworth, T., Petersen, R.G., 1985. Volume transport of the Antarctic circumpolar current from bottom pressure measurements. J. Phys. Oceanogr. 15, 810–816.

Whitworth, T., Nowlin, W.D., Worley, S.J., 1982. The net transport of the Antarctic Circumpolar Current through Drake Passage. J. Phys. Oceanogr. 12, 960–971.

Wunsch, C.W., Roemmich, D., 1985. Is the North Atlantic in Sverdrup balance? J. Phys. Oceanogr. 15, 1876–1880.

Young, W.R., 1981. A theory of the wind-driven circulation. Ph.D. thesis, MIT/WHOI Joint Program in Oceanography, 215 pp.